

We are IntechOpen, the world's leading publisher of Open Access books Built by scientists, for scientists

6,900

Open access books available

186,000

International authors and editors

200M

Downloads

Our authors are among the

154

Countries delivered to

TOP 1%

most cited scientists

12.2%

Contributors from top 500 universities



WEB OF SCIENCE™

Selection of our books indexed in the Book Citation Index
in Web of Science™ Core Collection (BKCI)

Interested in publishing with us?
Contact book.department@intechopen.com

Numbers displayed above are based on latest data collected.
For more information visit www.intechopen.com



Design and Modeling of WDM Integrated Devices Based on Photonic Crystals

Kiazand Fasihi
Golestan University
Iran

1. Introduction

Recently, photonic crystals (PCs) have attracted great interests due to their potential ability of controlling light propagation with the existence of photonic bandgap (PBG), and the possibilities of implementing compact nanophotonic integrated circuits. Some of the most successful structures are based on planar PCs. In such structures, the optical field is confined, horizontally, by a PBG provided by the PC and, vertically, by total internal reflection due to refractive index differences. Various PC components, such as, waveguides, bends, Y splitters, directional couplers, low crosstalk intersections and all-optical switches have already been realized. These basic building blocks can be combined to realize complete circuits with various optical functions within an extremely small area. One of the most important fields for ultra-dense integrated circuits is optical communications. A key component in modern optical communications systems is a wavelength division multiplexer (WDM). This component is needed to divide and combine different wavelength channels each carrying an optical data signal. Traditionally, WDM components are realized using thin-film filters, fiber Bragg gratings (FBG), or arrayed waveguide gratings. However, such devices are not convenient for ultra-dense integration. Various concepts for realizing a WDM component utilizing the extraordinary properties of PCs have recently been proposed. These ideas include optical micro-cavities, multimode self-imaging waveguides, and superprisms, but we focus on the components which are based on the interaction of the PC micro-cavities with the waveguides.

The chapter is organized as follows: In Section 2, the hybrid waveguides are introduced and analyzed using coupled-mode theory (CMT) and the finite-difference time-domain (FDTD) methods. First, the resonance frequencies and the field distribution of the resonance modes have been analyzed, then the hybrid waveguides are introduced and analyzed using FDTD and CMT methods, and the conditions which lead to quasi-flat and Lorentzian transmission spectrum will be presented. Finally, the Fundamental approach to low cross-talk and wideband intersections design which is based on the orthogonal hybrid waveguides is presented and analyzed using CMT and FDTD methods. It will be shown that when the phase-shift of the electromagnetic waves traveling between two adjacent PC coupled cavities is approximately equal to $(k + 1 / 2)\pi$, the best performance for the intersection can be achieved. In addition it will be shown that simultaneous crossing of ultra-short pulses is

possible. In Section 3, a three-port high efficient CDF with a coupled cavity-based wavelength-selective reflector is introduced and analyzed. According to the theoretical theory using CMT in time, the performance of the proposed CDF will be investigated and the conditions which lead to 100% drop efficiency will be extracted. The performance of the designed filter will also be calculated using the 2D-FDTD method. The simulation results show that the designed CDF has a line-width of $0.78nm$ at the center wavelength $1550nm$, and also a multi-channel CDF with channel spacing around $10nm$ ($1nm$) with inter-channel crosstalk below $-30dB$ ($-15dB$) is possible. These characteristics make the proposed CDF suitable for use in WDM optical communication systems.

2. Photonic crystal hybrid waveguides: Design and modeling

As mentioned before, PCs have gained great interest due to the availability of high density integrated optical circuitry (Joannopoulos et al., 2008; Yanik et al., 2004; Niemi et al., 2006; Koshiba, 2001; Fasihi & Mohammadnejad, 2009a, 2009b; Mekis et al., 1999; Loncar et al., 2000; Martinez et al., 2003; Shin et al., 2004; Liu & Chen, 2004; Yanik et al., 2003). PC waveguides provide an efficient means of guiding light by allowing the realization of sharp optical bends (Mekis et al., 1996). By combining the PC waveguides with PC cavities, realization of compact optical filter designs is possible (Fan et al., 1999). If the cavities are brought close together, they will couple and light will propagate through evanescent wave coupling from one cavity to its neighbors. This new type of waveguide is called the coupled-cavity waveguide (CCW) or alternatively, a coupled-resonator optical waveguide (CROW) (Yariv et al., 1999) and has many interesting properties. With such waveguides, by appropriately positioning the coupled optical cavities, sharp bends are also possible. In this section, the hybrid waveguides based on combining of the CCWs and the conventional line defect waveguides proposed and modeled by using CMT and FDTD methods. PC hybrid waveguides are a key element in the construction of future integrated optical circuits. Orthogonal hybrid waveguide intersections are very good candidate for wideband and low cross-talk intersections, which are a crucial element in PC-based integrated circuits (Fasihi & Mohammadnejad, 2009a). In some applications, such as ultra-short pulse transmission and time delay lines, the transmission spectrum is designed to be quasi-flat. By increasing the confinement of the coupled cavities in hybrid waveguides, the continuous transmission band will be converted to a series of discrete bands with Lorentzian spectrum, which are useful for implementation of some optical devices, such as filters (Ding et al., 2009). In this section, both analytical and numerical approaches are used to design and modeling of the hybrid waveguides with quasi-flat and Lorentzian transmission spectrum.

2.1 Analysis of the PC cavity modes

When a local defect is created in a PC, e.g. by removing a single rod, a cavity is formed where light is confined in one or more bound states. Depending on the quality of the confinement, these states, or modes, exist only in a narrow frequency range. In general, a defect can have any shape or size; it can be made by changing the refractive index of a rod, modifying its radius, or removing a rod altogether (Villeneuve et al., 1996). The defect could also be made by changing the index or the radius of several rods. Here, we choose to modify the radius of a single rod. For ease of computation, we use a 2D-PC consisting of a

hexagonal lattice of dielectric rods in air. The rods have lattice constant a , radius $r = 0.20a$, and refractive index $n_{rod} = 3.4$. This structure prohibits propagation of TM light (in-plane magnetic field) in the frequency range 0.280 to 0.452 ($2\pi c/a$). To determine the PBG regions of the PC structure, the MIT Photonic-Bands package (<http://ab-initio.mit.edu/mpb>) is used. In order to couple energy into the cavity, it is necessary to transfer energy through the walls of the PC. Incident light can transfer energy to the resonant mode by the evanescent field across the array of rods. The setup is shown in Fig. 1. To compute the resonant frequencies, we consider a finite-sized 13×21 PC in which a single rod has been removed. We send a wide-spectrum plane wave pulse with TM polarization at the incident angle of around 15° respect to the z-axis. On the other side of the PC, the field amplitude is monitored at a short length, marked as "Monitor". This configuration facilitates identifying of the resonance peaks of transmission spectrum, especially in some degenerate states. In this configuration the excitation has a Gaussian profile centered at $\omega = 0.37 (2\pi c/a)$ and a width of $\Delta\omega = 0.6 (2\pi c/a)$ which extends beyond the edges of the PBG. The resonant frequencies of the cavities are plotted as a function of the cavity radius in Fig. 2. This figure shows that as the radius of the cavity is reduced to $0.15a$, due to the increasing perturbation, a resonant cavity mode appears at the bottom of the PBG (Villeneuve et al., 1996). As the cavity radius is further reduced, since the cavity involves removing dielectric material in the PC, based on perturbation theorem, a higher frequency resonant mode is obtained (Joannopoulos et al., 2008), and eventually reaches $\omega = 0.3953 (2\pi c/a)$ when the rod is completely removed. The corresponding electric-field (E_y) distributions of the resonant mode is shown in Fig. 3-(d) for the case $r_d = 0.1a$. We name this state as "monopole", because it has no nodal lines in the central (cavity) rod. By increasing the cavity radius to $0.25a$, three triply-degenerate dipole states appears at the top of the PBG (the field distributions are shown in Fig. 3-(a) for the case $r_d = 0.3a$).

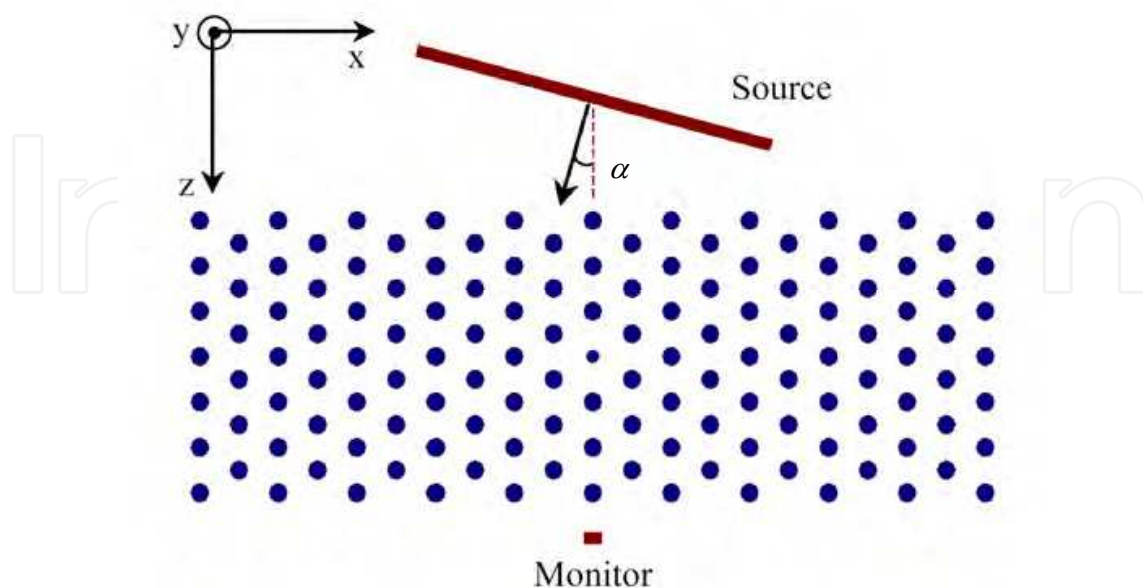


Fig. 1. The used set up for determining the resonance frequency of the cavity states in PC of hexagonal lattice.

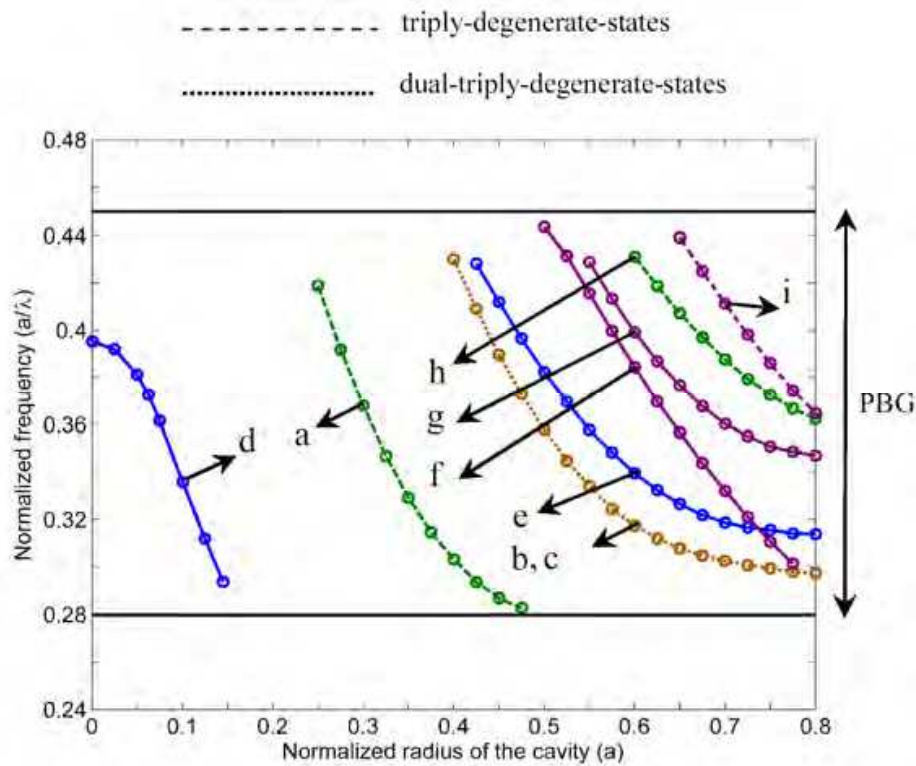
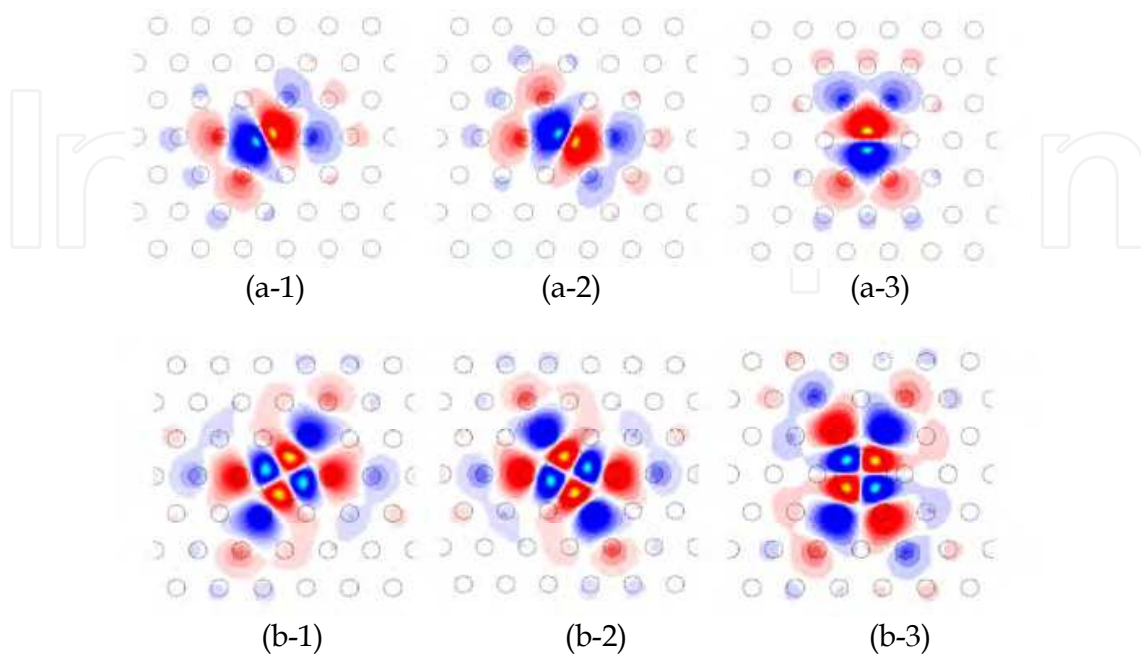


Fig. 2. The resonant frequencies for different cavities radius in the PC of hexagonal lattice.

These states named as a dipole to reflect the two lobes in their field distributions. If the radius is further increased then a sequence of higher-order modes (with more nodal planes) are pulled down into the PBG: six dual-triply-degenerate states (Fig. 3-(b), (c)), a higher-order monopole with an extra node in the radial direction (Fig. 3-(e)), a hexapole state and a second-order hexapole state (Fig. 3-(f), (g)), three triply-degenerate second order dipole states (Fig. 3-(h)), and three triply-degenerate octapole states (Fig. 3-(i)).



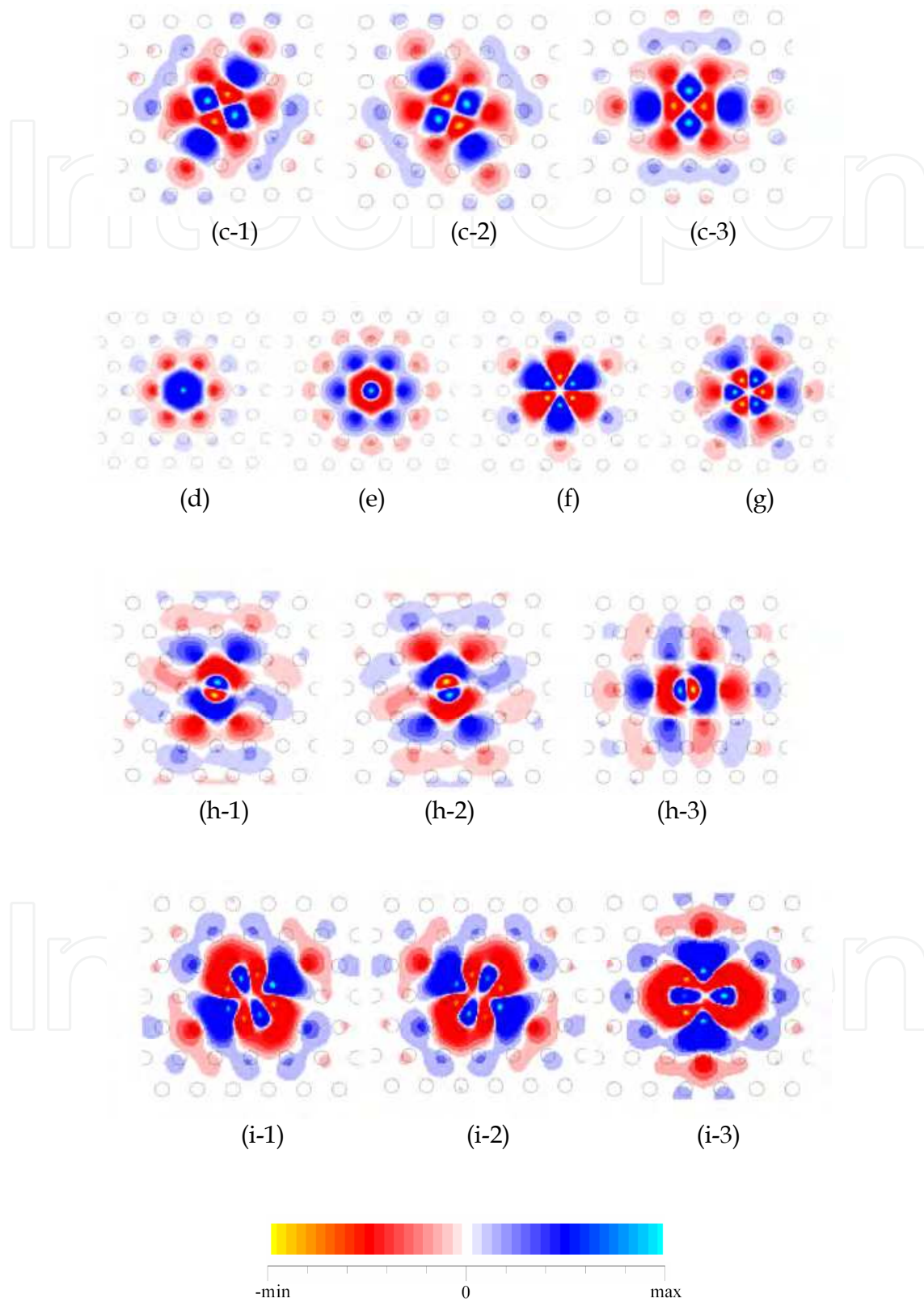


Fig. 3. The electric-field (E_y) distributions of the resonant modes for the labeled points of.

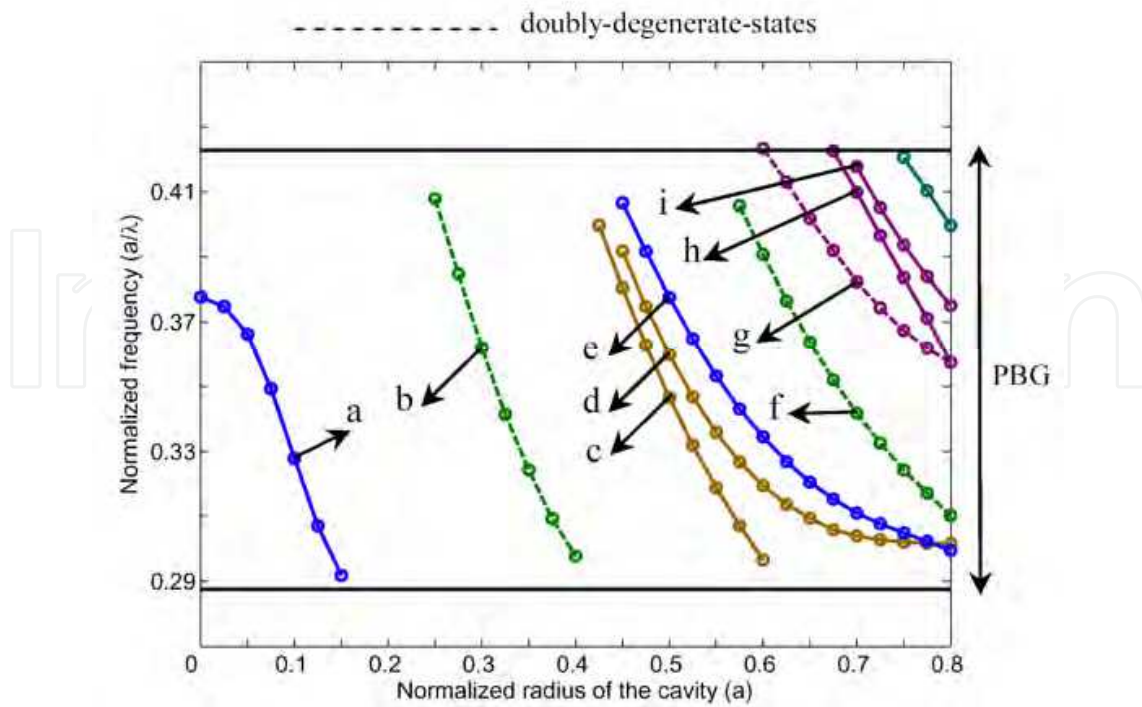
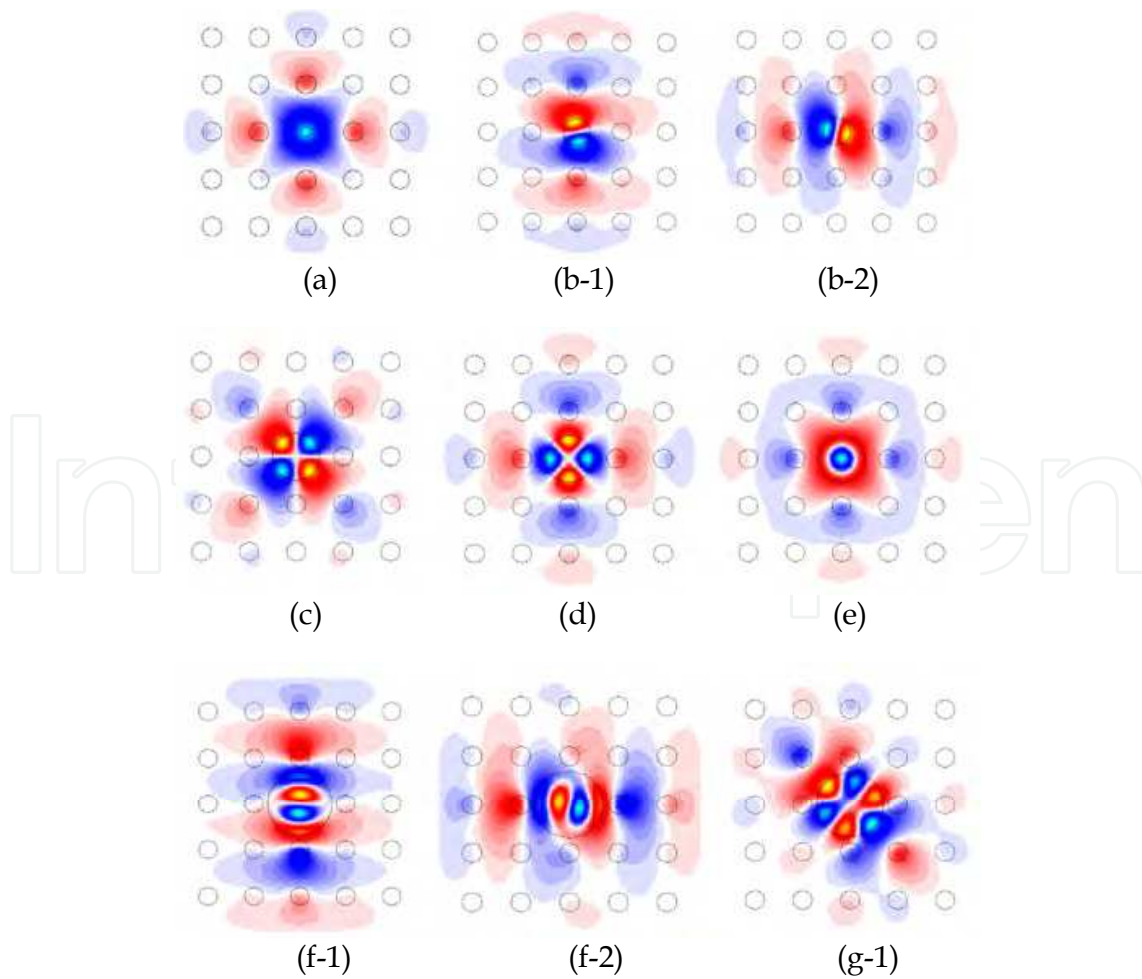


Fig. 4. The resonant frequencies for different cavities radius in the PC of square lattice.



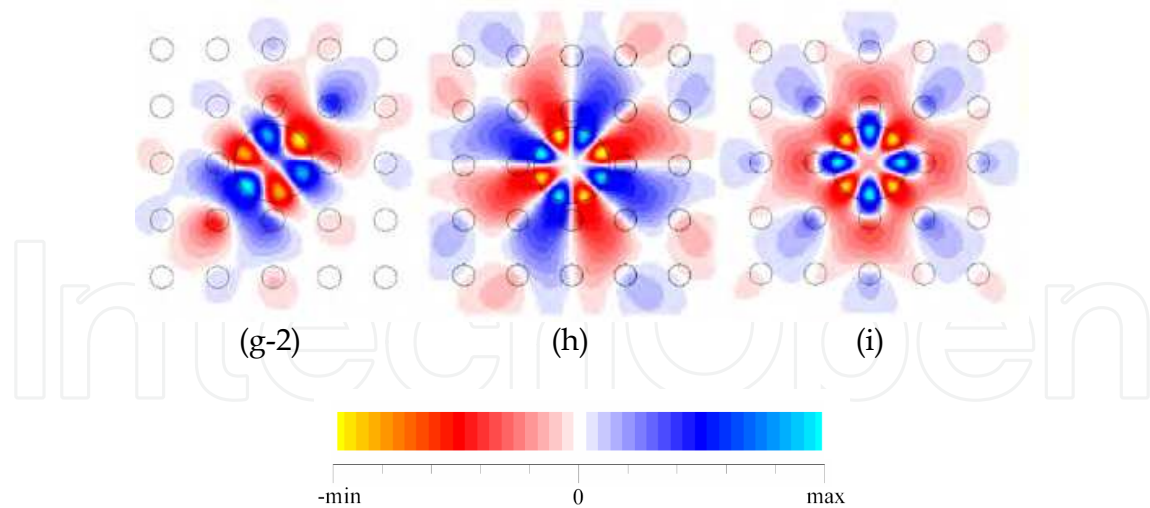


Fig. 5. The electric-field (E_y) distributions of the resonant modes for the labeled points of.

2.2 Analytical model for hybrid waveguides: CMT approximation

2.2.1 Hybrid waveguides

The PC based CCWs are formed by placing a series of high-Q optical cavities close together. In this case due to weak coupling of the cavities, light will be transferred from one cavity to its neighbors and a waveguide can be created (Yariv et al., 1999). By combining of the CCWs and the conventional line defect waveguides a new waveguide can be created, which is referred to as hybrid waveguide. Fig. 6 shows the structure of a hybrid waveguide which is implemented in a PC of square lattice. Generally, there are two types of PC lattice structures, air-hole-type and rod-type. Most theoretical studies conducted so far have investigated arrays of dielectric rods in air. The advantage of this model system is that waveguides created by removing a single line of rods are single moded. Getting light to travel around sharp bends with high transmission is then relatively straightforward, and many rod-type PC structures have been proposed. Such waveguides have been fabricated and photonic band gap guidance has been confirmed. Unfortunately, the rod in air approach does not provide sufficient vertical confinement and is difficult to implement in the optical regime.

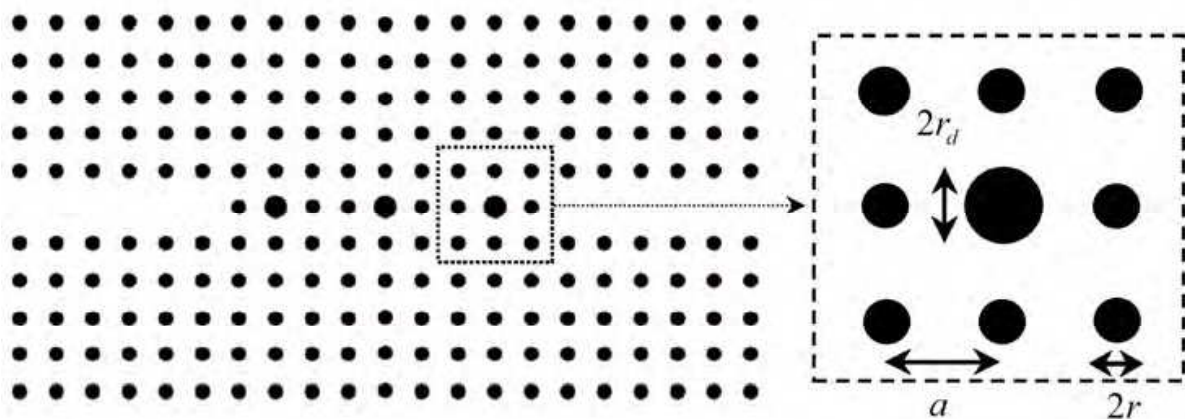


Fig. 6. Schematic of a PC hybrid waveguide of square lattice.

So, in practice, the PC slabs of dielectric rods in which the refractive index of the background material is higher than air, are used. Despite easier fabrication of PC waveguide based on air-hole-type structures than rod-type, there are limitations on frequency bandwidth of the single mode region and the group velocity (Fujisawa & Koshiba, 2006). Moreover in PC waveguides based on rod-type structure the large bandwidth and the large group velocity can be achieved, and recently such waveguides have been used for fabrication of photonic devices (Chen et al. 2005).

2.2.2 Modeling of hybrid waveguides by CMT method

Here, we consider the CCWs that are formed by periodically introducing defects along one direction in 2D-PCs. Generally, the coupling between two PC cavities depends on the leakage rate of energy amplitude into the adjacent cavity ($1/\tau$), which defines the quality factor of the cavity, and the phase-shift between two adjacent defects (φ). In a straight CCW which contains N PC cavities ($N > 3$), the transmission spectrum is given as (Sheng et al., 2005)

$$T_N = \left(\left[(\alpha^2 - \sin^2 \varphi) A_{N-2} - 2\alpha A_{N-3} + A_{N-4} \right]^2 \times (2 \sin \varphi)^{-2} + \left[-\alpha A_{N-2} + A_{N-3} \right]^2 \right)^{-1} \quad (1)$$

where

$$\alpha = 4Q(\omega / \omega_0 - 1) \sin \varphi - \cos \varphi, \quad Q = (\omega_0 \tau) / 4. \quad (2)$$

In the above equation, ω , ω_0 and Q are the frequency of incident input, the resonant frequency and the quality factor of the PC cavities, respectively. In (1), A is a series function of $\beta = (\alpha - \cos \varphi)$ that satisfies $A_{-1} = 0$, $A_0 = 1$ and $A_m = \beta A_{m-1} - A_{m-2}$ ($m = 1, 2, 3, \dots, N$). As shown in (1), apart from ω , the transmission spectrum of a CCW depends on three parameters ω_0 , Q and φ . The ω_0 and Q , can be extracted from a simple numerical simulation on a PC molecule, composed of two coupled cavities. For $N = 2$, i.e., a PC molecule, the transmission spectrum is given as

$$T_2 = \left(T_{\min}^{-1} - 8Q^2 \cos^2 \varphi \left(\frac{\omega}{\omega_0} - \frac{1}{4Q \tan \varphi} - 1 \right)^2 + 64Q^4 \sin^2 \varphi \left(\frac{\omega}{\omega_0} - \frac{1}{4Q \tan \varphi} - 1 \right)^4 \right)^{-1} \quad (3)$$

Where

$$T_{\min} = 4 \left(2 + \sin^{-2} \varphi + \sin^2 \varphi \right)^{-1}. \quad (4)$$

The parameter T_{\min} is the minimum in transmission band of a PC molecule. The peaks of the equation (3), which are equal to unity, appear at $\omega = \omega_0$ and $\omega = \omega_0 \left[1 + (2Q \tan \varphi)^{-1} \right]$. Hence, using (4) and the simulated transmission spectrum of one PC molecule, ω_0 and Q can be extracted. It must be noted that the analytical results of equation (1) can be extended to CCWs of any dimensions (Sheng et al., 2005). Now, we consider the hybrid waveguides that contain N identical cavities in 2D-PCs and generalize CMT analytical method to obtain

the transmission spectrum. According to (1), it can be seen that for a given N , the transmission spectrum curve has $2N - 1$ number of extremums and the minimum in transmission band (T_{\min}), is independent of ω_0 and Q , and we can obtain φ as a function of the radius of the coupled cavities (r_d), as follows (Fasihi & Mohammadnejad, 2009a):

- The relationship between T_{\min} and r_d can be calculated by repeating a numerical simulation, such as FDTD method, for different values of r_d .

Here we consider a hybrid waveguide which contains three coupled cavities, $N = 3$ (see Fig. 6), in the 2D-PC of square lattice composed of dielectric rods in air. Now, we have chosen to name this hybrid waveguide HW3 and extend this naming to other hybrid waveguides. The rods have refractive index $n_{rod} = 3.4$ and radius $r = 0.20a$, where a is the lattice constant. By normalizing every parameter with respect to the lattice constant a , we can scale the waveguide structure to any length scale simply by scaling a . The radius of the coupled cavities are varied from $0.27a$ to $0.345a$. The grid size parameter in the FDTD simulation is set to $0.046a$ and the excitations are electromagnetic pulses with Gaussian envelope, which are applied to the input port from the left side. All the FDTD simulations below are for TM polarization. The field amplitude is monitored at suitable location at the right side of the HW3. Table 1 shows the relationship between T_{\min} and r_d for the HW3 which are obtained from the FDTD simulations.

- The relationship between T_{\min} and φ for the HW3 can be calculated from (1).
- Fig. 7 shows this relationship over one-half period of (1). Therefore, the relationship between φ and r_d of the HW3 can be demonstrated in Fig. 8.

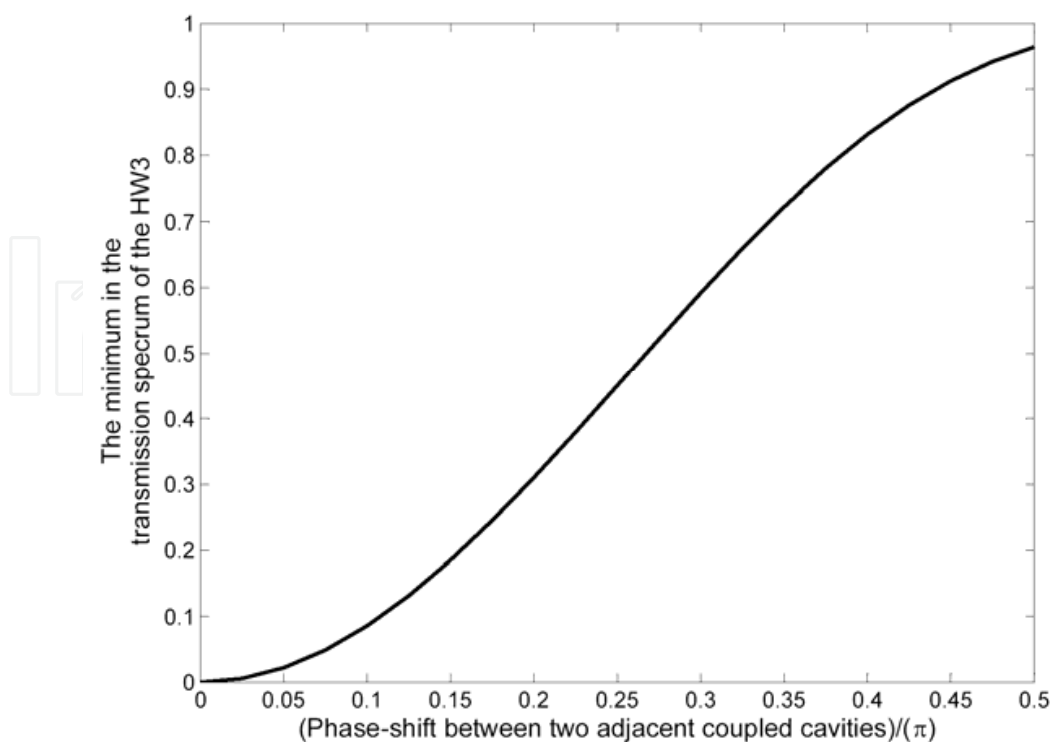


Fig. 7. The relationship between φ and T_{\min} of the HW3.

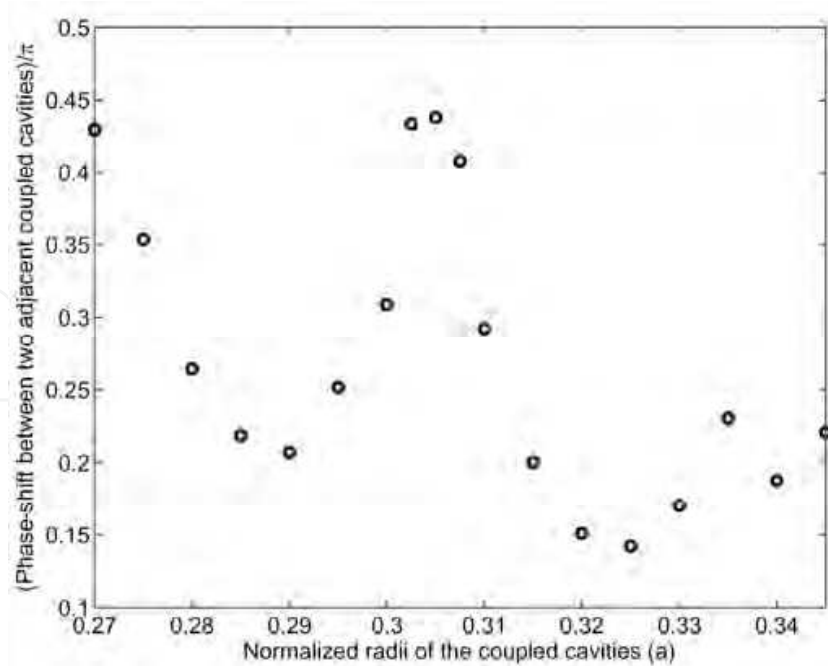


Fig. 8. The phase-shift between two adjacent cavities as a function of the cavities radius of the HW3 in a PC of square lattice (Fasihi & Mohammadnejad, 2009a).

r_d	T_{\min}	r_d	T_{\min}
0.270a	0.8831	0.3075a	0.8463
0.275a	0.7311	0.310a	0.5700
0.280a	0.4911	0.315a	0.3112
0.285a	0.3619	0.320a	0.1870
0.290a	0.3297	0.325a	0.1669
0.295a	0.4552	0.330a	0.2334
0.300a	0.6170	0.335a	0.3997
0.3025a	0.8894	0.340a	0.2773
0.3050a	0.8958	0.345a	0.3681

Table 1. Values of the Minimum in the HW3 Transmission Band for Various Radii of the Coupled Cavities

In order to compare the results of CMT and FDTD methods, we consider a HW2 under the same conditions as mentioned previously and utilize the FDTD simulation results to compute ω_0 and Q . The radius of the coupled cavities are set to $r_d = 0.32a$. The transmission spectrum of HW2 computed by the FDTD is shown in Fig. 9. According to this figure, the parameters ω_0 , Q and φ are equal to $0.3428 (2\pi c/a)$, 130.3 and 0.4066π , respectively. Hence, the CMT transmission spectrum can be calculated from (3) (see Fig. 9). It is observed that the transmission spectrum calculated by CMT is in good agreement with that simulated by FDTD. As another example, we take a HW3 under the same condition as mentioned previously, with $r_d = 0.32a$ which corresponds to $\varphi = 0.1509\pi$. The transmission spectra of the above HW3 simulated by FDTD and CMT are shown in Fig. 10 for comparison. Although there is a difference in the minimum transmission spectrum between

the first and second peaks, it is observed that the spectrum calculated by analytical method is nearly in good agreement with that simulated by the numerical simulation. Now, we consider a hybrid waveguide which contains three coupled cavities, in the 2D-PC of hexagonal lattice composed of dielectric rods in air. All conditions are the same as the previous structure and the radius of the coupled cavities is varied from 0 to $0.08a$. The relationship between φ and r_d of the HW3 in PC of hexagonal lattice is shown in Fig. 11. Tables 2 and 3 show the transmission regions and $-3dB$ bandwidths (BW) of the proposed hybrid waveguide for different values of the coupled cavities radii in PC of square and hexagonal lattices, respectively.

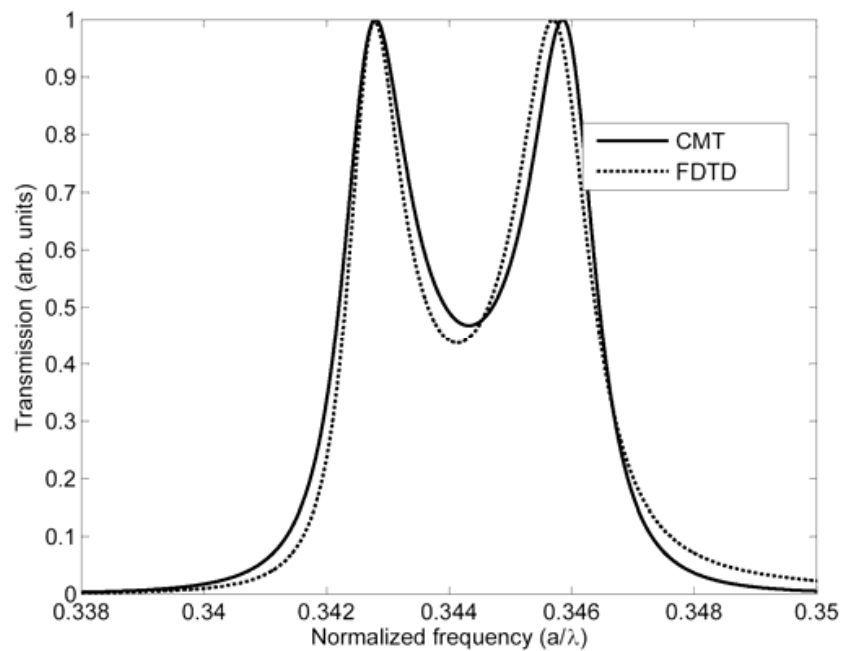


Fig. 9. The simulation results of transmission spectrum of the HW2 in PC of square lattice obtained by FDTD and CMT methods (Fasihi & Mohammadnejad, 2009a).

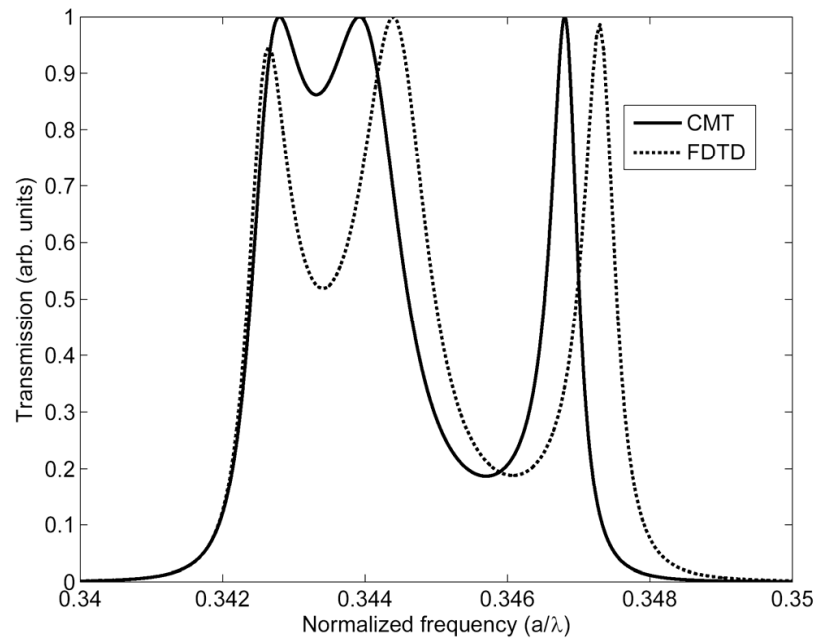


Fig. 10. The simulation results of transmission spectrum of the HW3 in PC of square lattice obtained by FDTD and CMT methods (Fasihi & Mohammadnejad, 2009a).

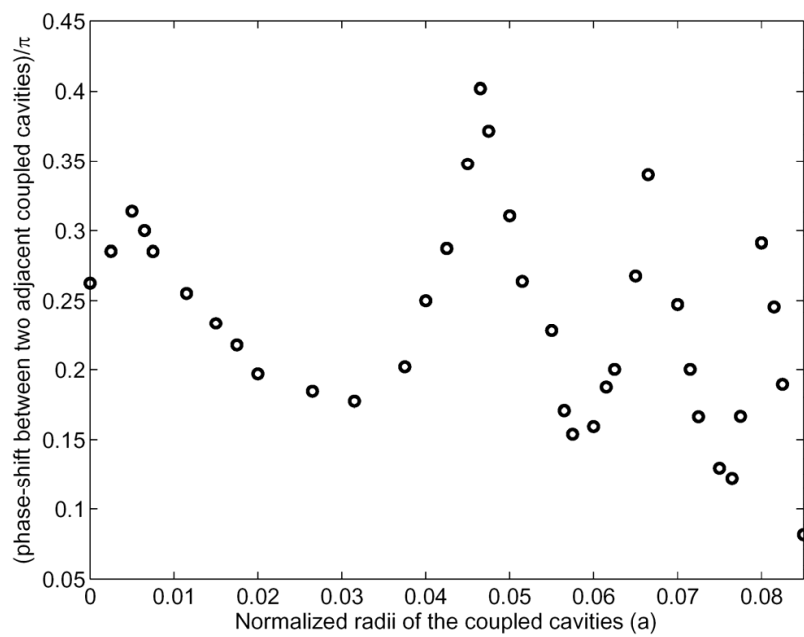


Fig. 11. The phase-shift between two adjacent cavities as a function of the cavities radius of the HW3 in a PC of hexagonal lattice.

Radius of cavities	Transmission region($2\pi c/a$)	-3dB BW (in terms of wavelength)	-3dB BW for $\alpha=0.55\mu\text{m}$
0.27a	0.3861-0.3932	0.0468a	25.7 nm
0.28a	0.3769-0.3829	0.0415a	22.8 nm
0.29a	0.3680-0.3734	0.0393a	21.6 nm
0.30a	0.3592-0.3645	0.0404a	22.2 nm
0.3025a	0.3569-0.3624	0.0425a	23.4 nm
0.3050a	0.3545-0.3601	0.0438a	24.1 nm
0.3075a	0.3522-0.3579	0.0452a	24.9 nm
0.31a	0.3503-0.3555	0.0417a	22.9 nm
0.32a	0.3423-0.3450	0.0228a	12.5 nm
0.33a	0.3348-0.3381	0.0291a	16.0 nm
0.34a	0.3272-0.3305	0.0305a	16.8 nm

*Assuming the lattice constant $\alpha=0.55\mu\text{m}$ considering that in this case the center wavelength of transmission band is equal to 1550nm when $r_d=0.3075\alpha$, the intersection BWs for different radius of the coupled cavities at working wavelength of 1550nm can be obtained and is shown in the column 4.

Table 2. Values of the Transmission Region and -3dB BW of the HW3 for Various Radiuses of the Coupled Cavities in PC of square lattice

Radius of cavities	Transmission region ($2\pi c/a$)	-3dB BW (in terms of wavelength)	-3dB BW for $\alpha=0.5937\mu\text{m}$
0	0.3954-0.3968	0.0143a	8.4 nm
0.005a	0.3929-0.3964	0.0223a	13.2 nm
0.010a	0.3926-0.3961	0.0222a	13.1 nm
0.015a	0.3930-0.3954	0.0149a	8.8 nm
0.020a	0.3924-0.3945	0.0136a	8.0 nm
0.025a	0.3914-0.3923	0.0059a	3.5 nm
0.030a	0.3901-0.3911	0.0063a	3.7 nm
0.035a	0.3886-0.3896	0.0065a	3.8 nm
0.040a	0.3864-0.3885	0.0135a	8.0 nm
0.045a	0.3829-0.3861	0.0219a	13.0 nm
0.0465a	0.3822-0.3854	0.0220a	13.1 nm
0.0475a	0.3814-0.3846	0.0221a	13.1 nm
0.050a	0.3791-0.3823	0.0223a	13.2 nm
0.055a	0.3751-0.3778	0.0089a	5.3 nm
0.060a	0.3738-0.3744	0.0042a	2.5 nm
0.065a	0.3694-0.3720	0.0186a	11.0 nm
0.070a	0.3642-0.3653	0.0083a	4.9 nm
0.075a	0.3607-0.3615	0.0060a	3.5 nm

** Assuming the lattice constant $\alpha=0.5937\mu\text{m}$ considering that in this case the center wavelength of transmission band is equal to 1550nm when $r_d=0.0475\alpha$, the intersection BWs for different radius of the coupled cavities at working wavelength of 1550nm can be obtained and is shown in the column 4.

Table 3. Values of the Transmission Region and -3dB BW of the HW3 for Various Radiuses of the Coupled Cavities in PC of hexagonal lattice

2.3 Design of hybrid waveguides with quasi-flat transmission spectrum

As discussed earlier, usually, the transmission spectrum is designed to be quasi-flat within the transmission region for various applications, such as ultra-short pulse transmission and also time delay lines. By comparing the results of Fig. 8 and Table 2, and also the results of Fig. 11 and Table 3, it can be seen that the optimum values of bandwidth is obtained when the phase-shift between two adjacent cavities are close to $\pi/2$ (rad). In this case, the transmission spectrum of the HW3 is quasi-flat. Fig. 12 shows the FDTD simulation results of the HW3 transmission spectrum (in PC of square lattice) for different radii, in which the phase-shift between the adjacent cavities is nearly $\pi/2$ (rad).

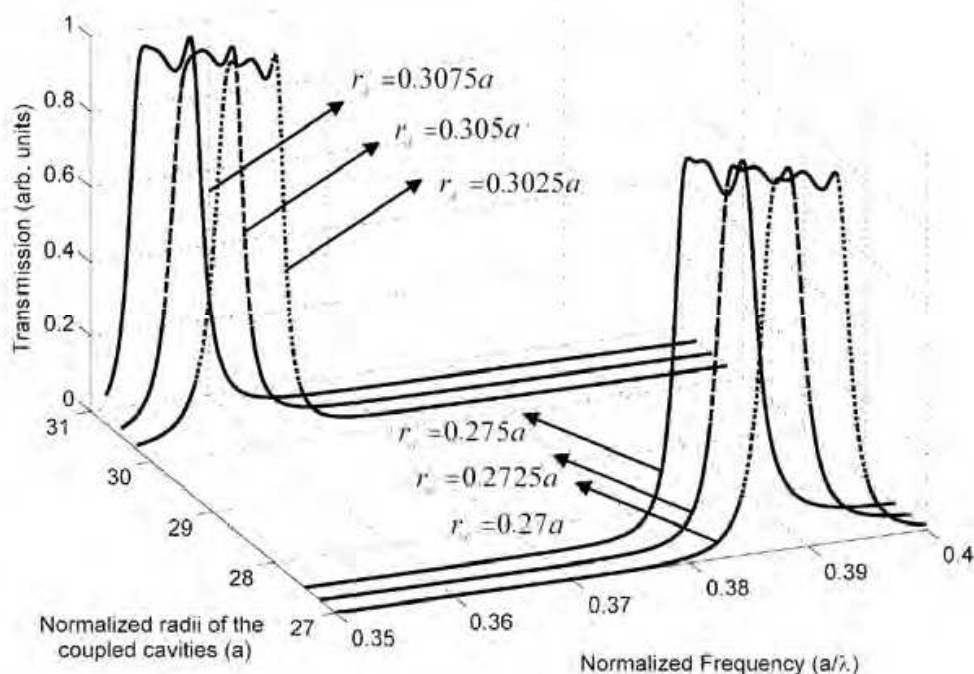


Fig. 12. The transmission behavior of the HW3 in a PC of square lattice when $\varphi \approx (k + 1/2)\pi$.

2.4 Design of hybrid waveguides with Lorentzian transmission spectrum

Using (1), it can be shown that the transmission spectrum is Lorentzian if the phase-shift between the adjacent cavities is close to 0 or π . Fig. 8 shows that for different radii of the coupled cavities, the phase-shift between the adjacent cavities isn't close to zero, hence we have a continuous transmission spectrum. By increasing the confinement of the coupled cavities, the continuous transmission spectrum tends to reduce into a series of discrete modes, which are useful for some optical devices, such as the WDM filters. To do this, we place two extra rods in both ends of the CCW. We consider the structure shown in Fig. 13, and investigate the effect of increasing confinement on transmission property with locating extra rods with radius of $0.2a$. All conditions are the same as the previous structure studied at section 3.2 and the radius of the coupled cavities is varied from 0 to $0.08a$. Fig. 14 shows the relationship between φ and r_d of the modified HW3 with Lorentzian spectrum. The

FDTD simulation results of the modified HW3 transmission spectrum for different radii, in which the phase-shift between the adjacent cavities is nearly zero, is shown in Fig. 15.

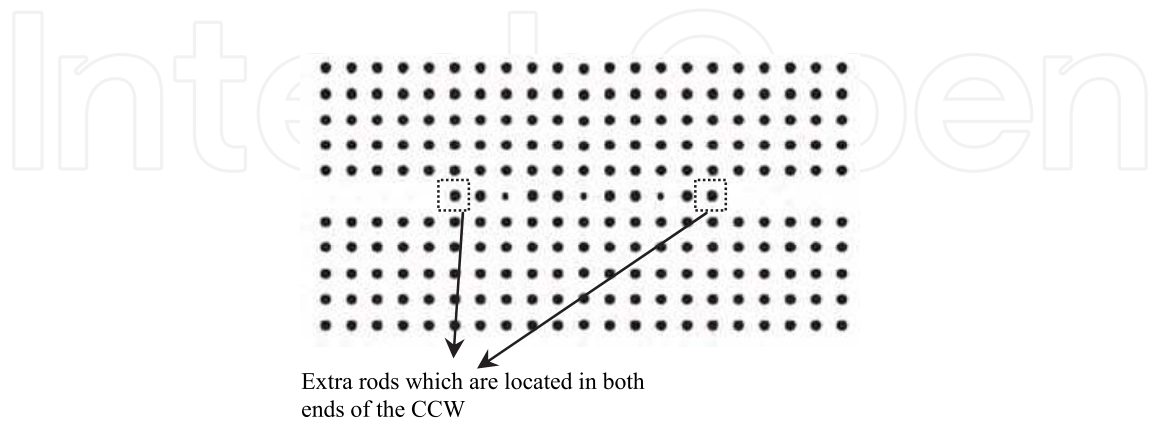


Fig. 13. The modified HW3 in a PC of square lattice with Lorentzian transmission spectrum.

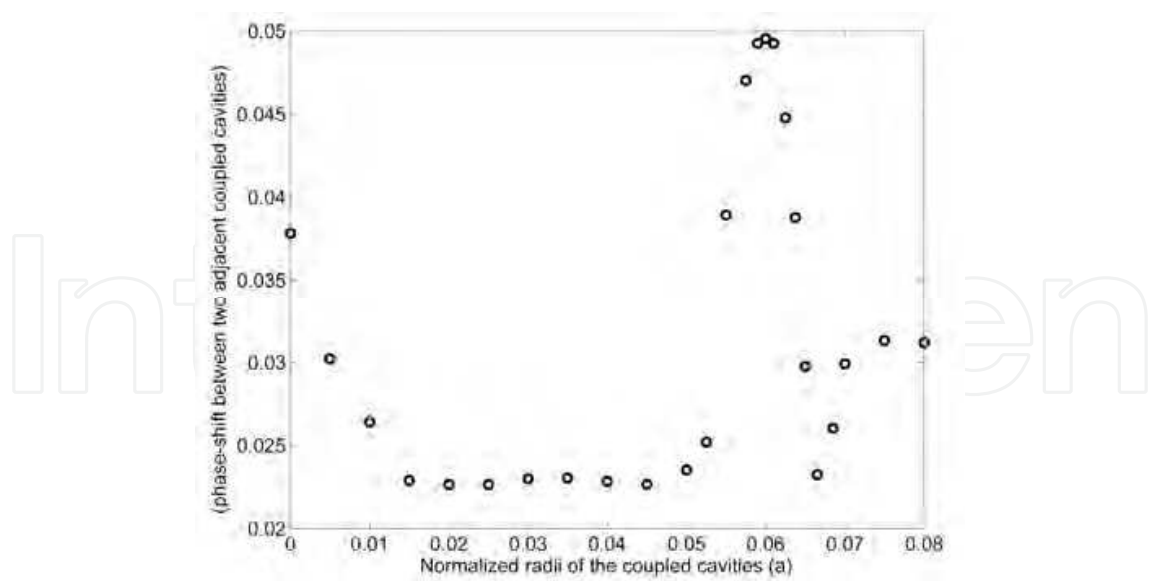


Fig. 14. The phase-shift between two adjacent cavities as a function of the cavities radius of the modified HW3 in a PC of square lattice.

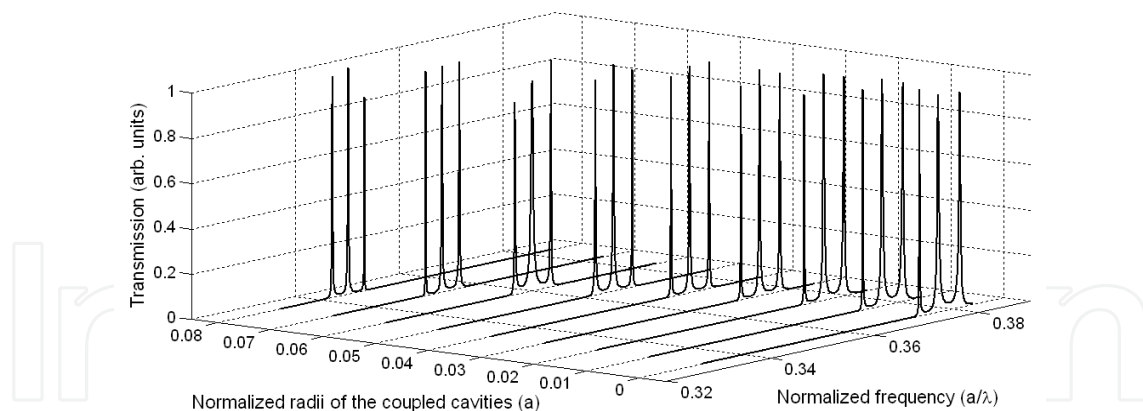


Fig. 15. The transmission behavior of the modified HW3 in a PC of square lattice when $\varphi \approx 0$.

2.5 Orthogonal hybrid waveguides: An approach to low cross-talk and wideband intersection design

In the implementation of PC-based integrated circuits, such as those used in WDM systems, it is necessary to have intersections in which crossing of ultra-short lightwave signals are possible. In another study, we show that the orthogonal hybrid waveguide intersections are very good candidate for wideband and low cross-talk intersections, which are a key element in PC-based integrated circuits (Fasihi & Mohammadnejad, 2009a). In 1998 Johnson et al. proposed a scheme to eliminate cross-talk for a waveguide intersection based on a 2D-PC of square lattice by using a single defect with doubly degenerate modes (Johnson et al., 1998). They also presented general criteria for designing such waveguide intersections based on symmetry consideration. Lan and Ishikawa presented another mechanism where the defect coupling is highly dependent on the field patterns in the defects and the alignment of the defects (i.e., the coupling angle) (Lan & Ishikawa, 2002). They asserted that their design leads to a 10 nm wide region at the central wavelength of 1310 nm with cross-talk as low as -10 to -45 dB, while in Ref. (Johnson et al., 1998) the width of the transmission band with comparable cross-talk is only 7.8 nm. In the above mentioned design, the central wavelength value of the low cross-talk transmission band is related to the air-holes radii of PC structure and therefore, adjusting the wavelength domain of transmission band is a challenge. Furthermore, Liu et al. proposed another waveguide intersection for lightwaves with no cross-talk and excellent transmission which was based on non-identical PC coupled resonator optical waveguide (CROW), without transmission band overlap (Liu et al., 2005). Li et al. proposed a different approach that utilizes a vanishing overlap of the propagation modes in the waveguides created by line defects which support dipole-like defect modes (Li et al., 2007). They claimed that in their design, over a BW of 30 nm with the central wavelength at 1300 nm, transmission efficiency above 90% with cross-talk below -30 dB can be obtained. It is obvious that in that proposal - and also in (Liu et al., 2004), simultaneous propagation of lightwaves with equal frequencies through the intersection is impossible and due to using of taper structure to solve the mode mismatch problem, total length of the intersection is increased. In our solution an approach to design of low cross-talk and wideband PC waveguide intersections based on two orthogonal hybrid waveguides in a crossbar configuration, is proposed. Without losing generality, once again we consider a 2D square lattice of infinitely long dielectric rods in the air. Fig. 16 shows the structures of an orthogonal hybrid waveguide intersection in which the rods have refractive index $n_{rod} = 3.4$ and radius $r = 0.20a$.

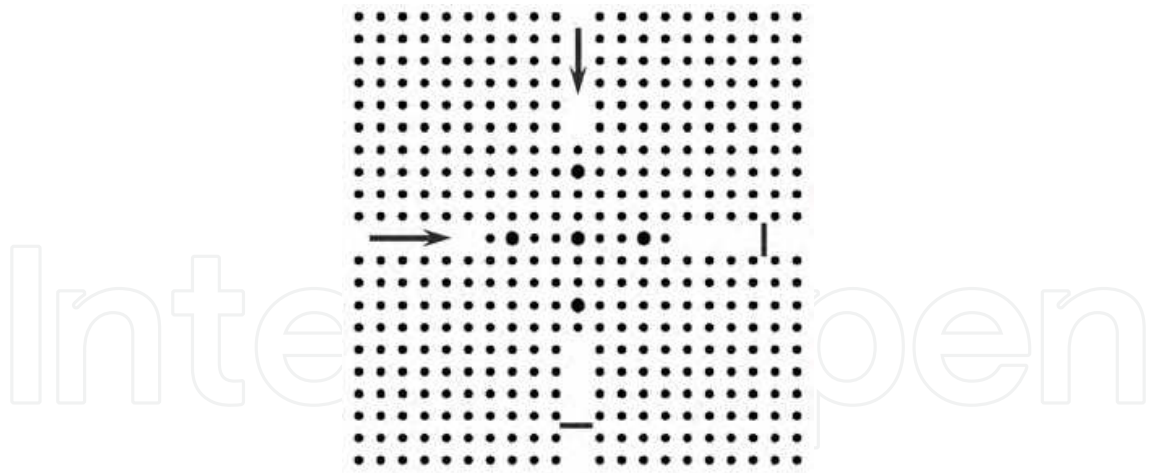
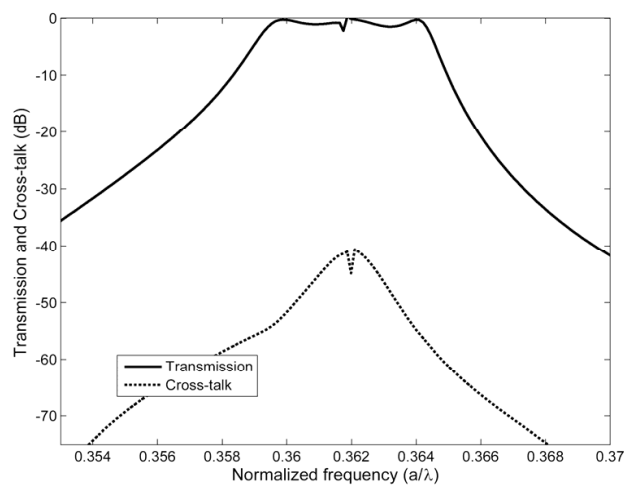
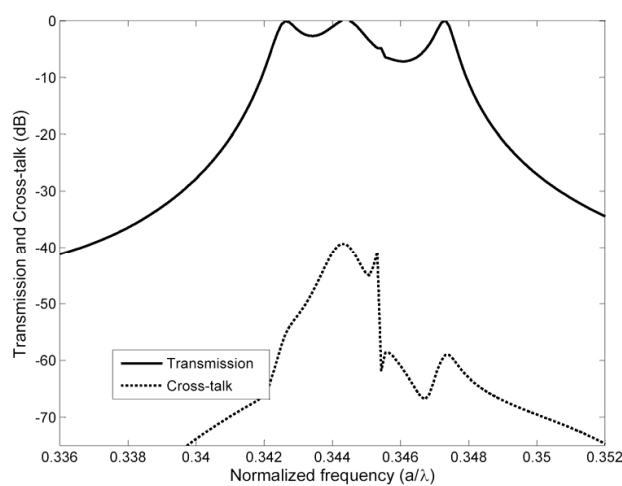


Fig. 16. Schematic structures of an orthogonal hybrid waveguide intersection.



(a)



(b)

Fig. 17. The transmission and cross-talk characteristics of the orthogonal HW3 intersection when the radius of the coupled cavities are set to (a) $r_d = 0.28a$ and (b) $r_d = 0.32a$ (Fasihi & Mohammadnejad, 2009a).

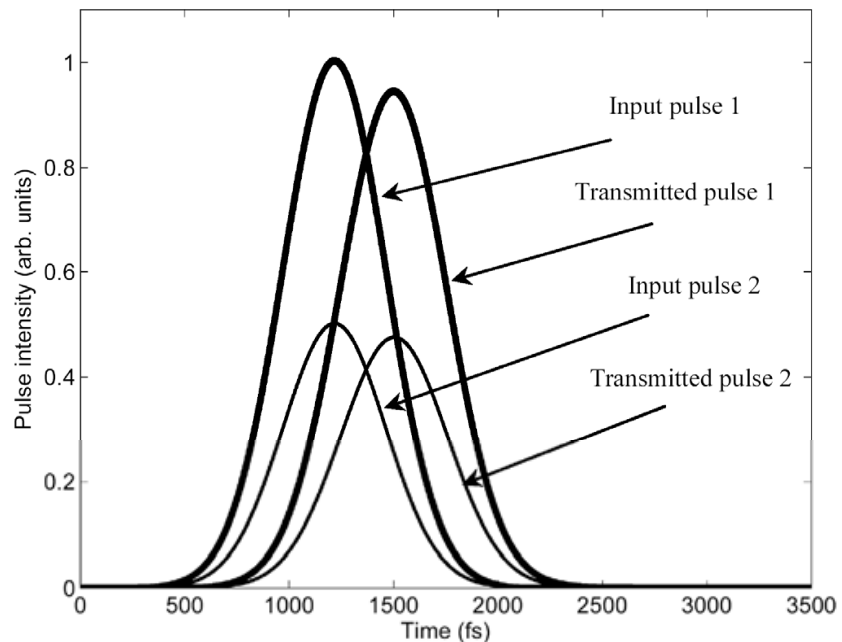
Radius of cavities	-3dB BW for $a = 0.55\mu\text{m}$	Cross-talk range (dB)	
0.27a	25.7 nm	-34.35	-41.74
0.28 a	22.8 nm	-32.16	-47.60
0.29 a	21.6 nm	-33.39	-52.76
0.30 a	22.2 nm	-40.19	-53.42
0.3025 a	23.4 nm	-43.96	-55.06
0.305 a	24.1 nm	-45.35	-55.05
0.3075 a	24.9 nm	-46.66	-56.23
0.31 a	22.9 nm	-46.16	-55.58
0.32 a	12.5 nm	-39.34	-59.21
0.33 a	16.0 nm	-35.61	-60.89
0.34 a	16.8 nm	-38.79	-50.27

Table 4. Values of -3dB BW and cross-talk in orthogonal HW3 intersection for various radii of the coupled cavities

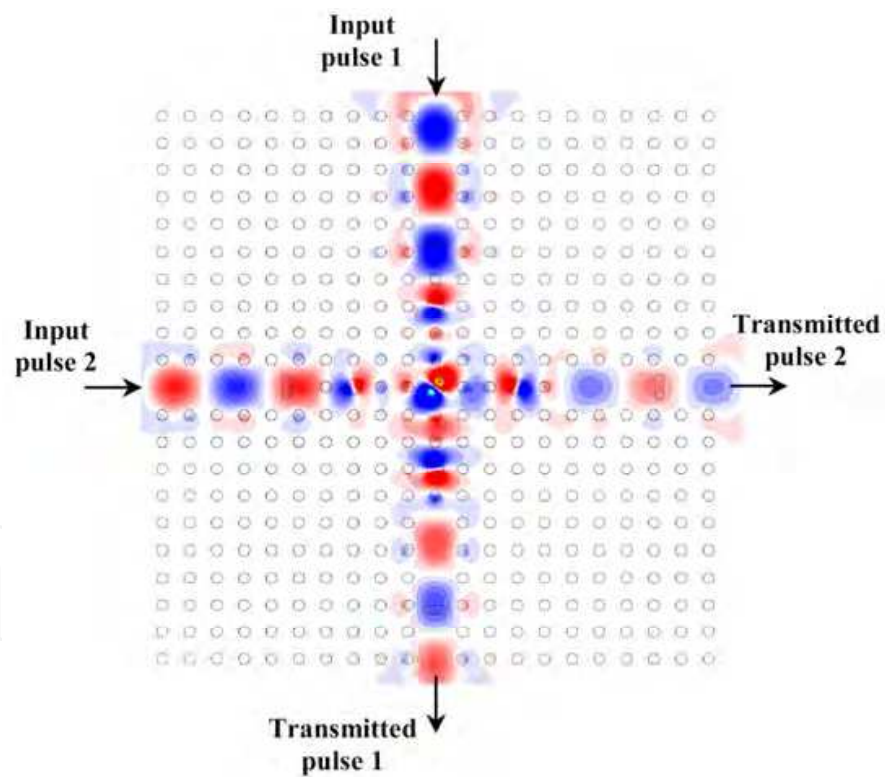
To evaluate the performance of the proposed device, the FDTD method is used for simulation, under the same conditions as mentioned previously. The excitations are electromagnetic pulses with Gaussian envelope, which are launched to the input port from the left side. The field amplitudes are monitored at suitable locations around the intersection in horizontal and perpendicular waveguides. Fig. 17-(a) and (b) shows the transmission and cross-talk characteristics of the orthogonal HW3 intersection, where the radius of the coupled cavities are set to $r_d = 0.28a$ and $r_d = 0.32a$, respectively. As can be seen from Fig. 17-(a) and (b), there exists around $0.0415a$ and $0.0228a$ regions in which the transmission is over 50%. Also, it must be noted that the transmission properties of the proposed intersection are the same as transmission properties of the corresponding hybrid waveguide. Furthermore, by varying the radius of the coupled cavities of the hybrid waveguides, a wide frequency domain of transmission band will be obtained which proves the flexibility of the proposed design. Table II shows -3 dB BW and the cross-talk of the proposed intersection for different values of the coupled cavities radii. By comparing the results of Fig. 8 and Table 4, it can be seen that the optimum values of BW and cross-talk are obtained when $\varphi \approx (k + 1/2)\pi$. In this case, the transmission spectra of the intersection is quasi-flat (see Fig. 12).

2.5.1 Simultaneous crossing of lightwave signals and transmission of ultra-short pulses through the orthogonal hybrid waveguide intersections

In the implementation of PC-based integrated circuits, it is necessary to have intersections in which simultaneous crossing of lightwaves is possible. In the orthogonal hybrid waveguide intersections, lightwave signals can cross through the intersection simultaneously because each resonant state of the intersection will couple to modes in just one waveguide and be orthogonal to modes in the other waveguide. We consider the structure shown in Fig. 16 and verify this idea by using the FDTD technique. In this simulation, the radius of the coupled cavities of the orthogonal HW3 are chosen to be $r_d = 0.3075a$ where $a = 0.55\mu\text{m}$. During simulation, two input pulses with Gaussian envelope are applied to input ports from the top and the left sides. The monitors are placed at right and bottom output ports at suitable locations. The intensities of 500-fs pulses are adjusted to unity and 0.5, while their central wavelengths are set at 1550nm and the phase difference between them is 180° . Fig. 18 shows the transmission



(a)



(b)

Fig. 18. The simultaneous crossing of two lightwave signals through the orthogonal HW3 intersection with $r_d = 0.3075a$ and $a = 0.55\mu m$. (a) Calculated transmission spectra (b) Calculated field distribution. The intensities of 500-fs pulses are adjusted to unity and 0.5, while their central wavelengths are set at $1550nm$ and the phase difference between them is 180° . (Fasihi & Mohammadnejad, 2009a)

behavior of simultaneous crossing of lightwave signals through the orthogonal HW3 intersection. It can be seen that the input pulses are transmitted through the intersection with negligible interference effect. In a separate assessment, we again consider the structure shown in Fig. 16 with $r_d = 0.3075a$ where $a = 0.55\mu m$, and investigate the transmission property of the intersection for ultra-short pulses by using the FDTD method. Fig. 19 shows the transmission behavior of a 200-fs pulse whose central wavelength is $1550nm$. We can see that not only the cross-talk is negligible, but also the distortion of the pulse shape is very small.

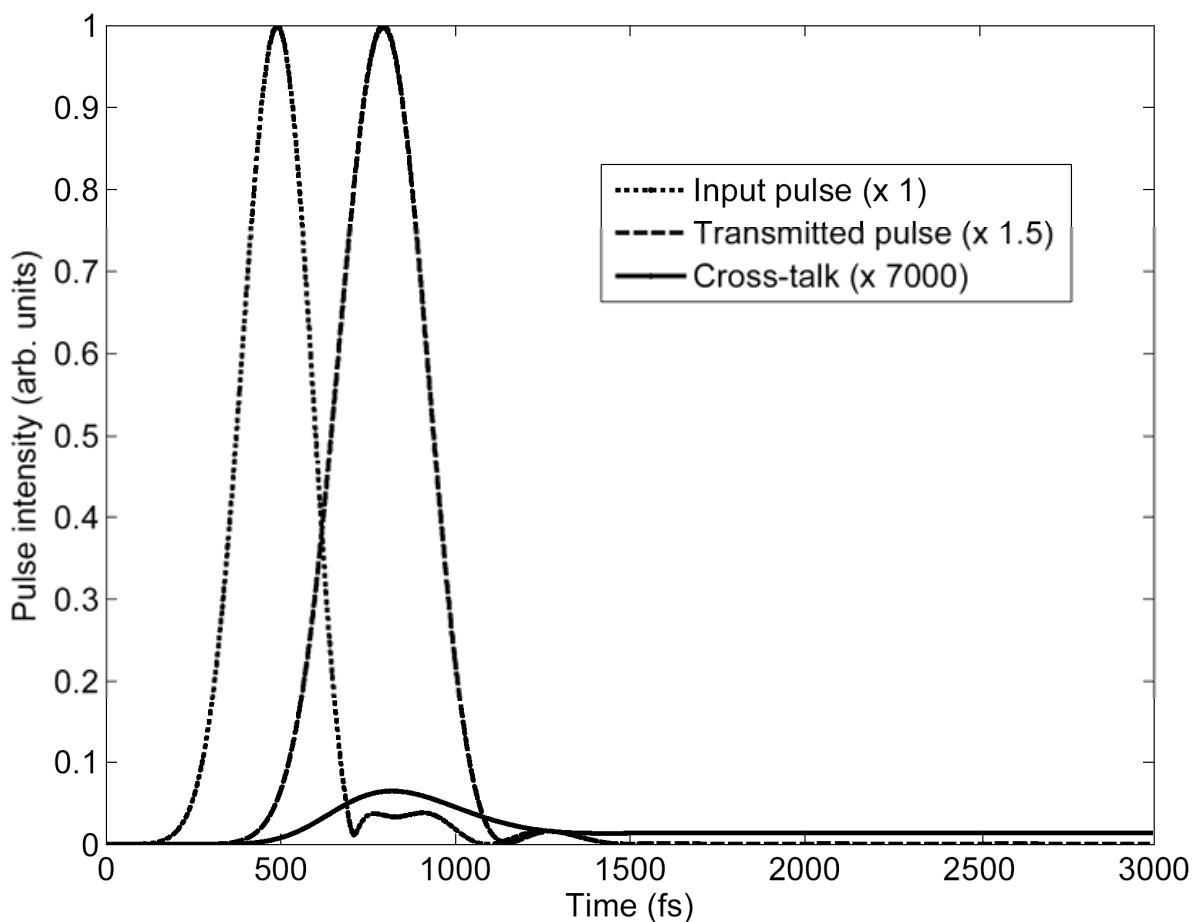


Fig. 19. The transmission behavior of a 200-fs pulse whose central wavelength is $1550nm$ through the orthogonal HW3 intersection with $r_d = 0.3075a$ and $a = 0.55\mu m$.

3. Highly efficient channel-drop filter with a coupled cavity-based wavelength-selective reflection feedback

The rapidly growing use of optical WDM systems, calls for ultra-compact and narrowband channel-drop filters (CDF). In a CDF, a single channel with a narrow linewidth can be selected, while other passing channels remain undisturbed. The means to control the propagation of light is mainly obtained by introducing defects in PCs. Microcavities formed by point defects and waveguides formed by line defects in PCs. In particular, the resonant CDFs implemented in PC, which are based on the interaction of

waveguides with micro-cavities, can be made ultra-compact and highly wavelength-selective (Zhang & Qiu, 2006). These devices attract strong interest due to their substantial demand in WDM optical communication systems. So far, different designs of CDFs in 2D-PCs have been proposed (Kim et al., 2007). These designs can be basically classified into two categories: surface emitting designs and in-plane designs. The surface emitting designs make use of side-coupling of a cavity to a waveguide. The input signal at resonant frequency tunnels from the waveguide into the cavity and is emitted vertically into the air (Noda et al., 2000; Song et al., 2005). The in-plane designs usually may be classified into two categories: four-port CDF designs and three-port CDF designs. The four-port CDF designs usually involve the resonant tunneling through a cavity with two degenerate modes of different symmetry, which is located between the two parallel waveguides (bus and drop). Although in this design a complete channel-drop transfer at resonant frequency is possible (i.e., 100% channel-drop efficiency), but enforcing degeneracy between the two resonant modes of different symmetry requires a complicated resonator design (Fan et al., 1998; Min et al., 2004). The operation principle of four-port CDF designs with and without mirror-terminated waveguides, have matured over the years (Zhang & Qiu, 2004). The basic concept of three-port CDF designs is based on direct resonant tunneling of input signal from bus waveguide to drop waveguide. This kind of CDF designs have simple structures and can be easily extended to design multi-channel drop filters (Kim et al., 2004), (Tekeste & Yarrison-Rice, 2006; Notomi et al., 2004). In a typical three-port CDF, the power transmission efficiency is inherently less than 50% (which corresponds the transmission in the resonant frequency), because a part of trapped signal in the cavity is reflected back to the bus waveguide when channel-drop tunneling process occurs. So far, different approaches have been proposed to solve this problem. Fan et al. proposed an approach to enhance the drop efficiency using controlled reflection to cancel the overall reflection in a full demultiplexer system. This structure is realized by coupling among an ultra low-quality factor cavity and micro-cavities with high-quality factor (Jin, 2003). Kim et al. proposed a three-port CDF with reflection feedback, in which nearly 100% drop efficiency can be theoretically achieved. In this design, the reflected back power to input port, except at the resonant frequencies, is close to 100% which leads to noise if the designed structure is incorporated in photonic integrated circuits (Kim et al., 2004). A similar design has also been proposed by Kuo et al. based on using high Q-value micro-cavities with asymmetric super-cell design (Kuo et al., 2006). This design leads to an improvement in the drop efficiency and the full-width at half-maximum (FWHM), respect to the corresponding symmetric super-cell. Another three-port CDF with a wavelength-selective reflection micro-cavity has been proposed by Ren et al. (Ren et al., 2006). In the proposed design two micro-cavities are used. One is used for a resonant tunneling-based CDF, and another is used to realize wavelength-selective reflection feedback. In this section we study a three-port system which is based on two coupled cavities in both drop and reflector sections. We show that the proposed structure can provide a practical approach to attain a high efficient CDF with narrow FWHM, with no reduction in transmission efficiency parameter. Here, we consider the structure shown in Fig. 20, where the coupled cavities of the drop and the reflector sections are located at opposite sides of the bus waveguide to prevent the direct coupling between them.

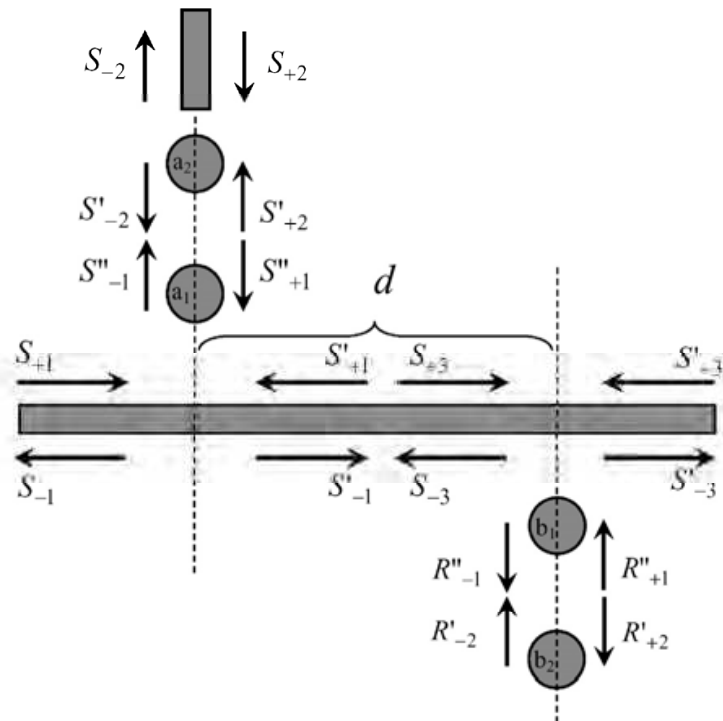


Fig. 20. The basic structure of the proposed three-port CDF with coupled cavity based wavelength selective-reflector (Fasihi & Mohammadnejad, 2009b).

The time evolution of the cavities modes, given that all of the cavities decay rates which are due to internal loss of energy be equal to τ_0 , are expressed by (Fasihi & Mohammadnejad, 2009b; Haus, 1984; Manolatu et al., 1999)

$$\frac{da_1}{dt} = j\omega_{\text{Res}-a}a_1 - a_1\frac{1}{\tau_0} - a_1\frac{2}{\tau_1} - a_1\frac{1}{\tau_2} + e^{j\theta_1}\sqrt{\frac{2}{\tau_1}}S_{+1} + \sqrt{\frac{2}{\tau_2}}S''_{+1} + e^{j\theta_1}\sqrt{\frac{2}{\tau_1}}S'_{+1} \quad (5)$$

$$\frac{da_2}{dt} = j\omega_{\text{Res}-a}a_2 - a_2\frac{2}{\tau_2} - a_2\frac{1}{\tau_0} + \sqrt{\frac{2}{\tau_2}}S'_{+2} + e^{j\theta_2}\sqrt{\frac{2}{\tau_2}}S_{+2} \quad (6)$$

$$\frac{db_1}{dt} = j\omega_{\text{Res}-b}b_1 - b_1\frac{1}{\tau_0} - b_1\frac{2}{\tau_3} - b_1\frac{1}{\tau_4} + e^{j\theta_1}\sqrt{\frac{2}{\tau_3}}S_{+3} + \sqrt{\frac{2}{\tau_4}}R''_{+1} \quad (7)$$

$$\frac{db_2}{dt} = j\omega_{\text{Res}-b}b_2 - b_2\frac{1}{\tau_4} - b_2\frac{1}{\tau_0} + \sqrt{\frac{2}{\tau_4}}R'_{+2} \quad (8)$$

Here, $\omega_{\text{Res}-a}$ and $\omega_{\text{Res}-b}$ are the resonant frequencies of the coupled cavities in the drop and the reflector sections, respectively, $1/\tau_1$ and $1/\tau_3$ denote the decay rates of cavities a_1 and b_1 into the bus waveguide, respectively, $1/\tau_2$ is the decay rate of cavities a_2 into the drop waveguide and also is the decay rates of the cavity a_2 into the cavity a_1 and vice versa, and $1/\tau_4$ is the decay rates of the cavity b_2 into the cavity b_1 and vice versa. As shown in Fig.

21, the amplitudes of the electromagnetic waves (EM) incoming the drop (reflector) section from the bus waveguide, are denoted by S_{+1} (S_{+3}) and S'_{+1} (S'_{+3}). Also, the amplitudes of the EM waves outgoing the drop (reflector) section to the bus waveguide, are denoted by S_{-1} (S_{-3}) and S'_{-1} (S'_{-3}). In the case of EM waves traveling between the coupled cavities, in the drop section, the EM wave incoming the cavity a_1 (a_2) is denoted by S''_{+1} (S'_{+2}), and the EM waves outgoing the cavity a_1 (a_2) is denoted by S''_{-1} (S'_{-2}), respectively, and in the reflector section, the EM wave incoming the cavity b_1 (b_2) is denoted by R''_{+1} (R'_{+2}), and the EM wave outgoing the cavity b_1 (b_2) is denoted by R''_{-1} (R'_{-2}), respectively. The relationships among the denoted EM waves amplitudes and the cavities mode amplitudes are

$$S'_{-3} = S_{+3} - \sqrt{\frac{2}{\tau_3}} e^{-j\theta_3} b_1 \quad (9)$$

$$S_{-3} = S'_{+3} - \sqrt{\frac{2}{\tau_3}} e^{-j\theta_3} b_1 \quad (10)$$

$$S'_{-1} = S_{+1} - \sqrt{\frac{2}{\tau_1}} e^{-j\theta_1} a_1 \quad (11)$$

$$S_{-1} = S'_{+1} - \sqrt{\frac{2}{\tau_1}} e^{-j\theta_1} a_1 \quad (12)$$

$$S_{-2} = -S_{+2} + \sqrt{\frac{2}{\tau_2}} e^{-j\theta_2} a_1 \quad (13)$$

$$S''_{-1} = -S''_{+1} + \sqrt{\frac{2}{\tau_2}} a_1 \quad (14)$$

$$S'_{-2} = -S'_{+2} + \sqrt{\frac{2}{\tau_2}} a_2 \quad (15)$$

$$R''_{-1} = -R''_{+1} + \sqrt{\frac{2}{\tau_4}} b_1 \quad (16)$$

$$R'_{-2} = -R'_{+2} + \sqrt{\frac{2}{\tau_4}} b_2 \quad (17)$$

$$S_{+3} = S'_{-1} e^{-j\beta d} \quad (18)$$

$$S'_{+1} = S_{-3} e^{-j\beta d} \quad (19)$$

In the above equations, θ_1 and θ_2 are the phases of the coupling coefficients between the bus waveguide and the cavities a_1 and b_1 , respectively, θ_3 is the phase of the coupling coefficient between the drop waveguide and cavity a_2 , β is the propagation constant of the bus waveguide, and d is the distance between two reference planes. The EM waves traveling between the two coupled cavities in drop and reflector sections, satisfy

$$S'_{+2} = S''_{-1} e^{-j\varphi} \quad (20)$$

$$S''_{+1} = S'_{-2} e^{-j\varphi} \quad (21)$$

$$R'_{+2} = R''_{-1} e^{-j\varphi} \quad (22)$$

$$R''_{+1} = R'_{-2} e^{-j\varphi}. \quad (23)$$

Based on Eqs. (16)-(17) and (22)-(23), when $\tau_3 = \tau_4$ we have

$$R''_{+1} = \sqrt{\frac{2}{\tau_4}} \left(\frac{b_2 - b_1 e^{-j\varphi}}{2j \sin \varphi} \right) \quad (24)$$

$$R'_{+2} = \sqrt{\frac{2}{\tau_4}} \left(\frac{b_1 - b_2 e^{-j\varphi}}{2j \sin \varphi} \right). \quad (25)$$

By substituting the Eqs. (24)-(25), in Eqs. (7)-(8), when EM wave is launched only from the left side into the bus waveguide ($S_{+2}, S'_{+3} = 0$), we find

$$S_{+3} = \frac{e^{-j\theta_3} \left[\gamma^2 - \frac{\tau_4}{\tau_0} \left(\frac{2\tau_4}{\tau_3} + \frac{\tau_4}{\tau_0} \right) \sin^2 \varphi - 1 - j\gamma \sin \varphi \left(\frac{2\tau_4}{\tau_3} + \frac{2\tau_4}{\tau_0} \right) \right]}{-j \sqrt{\frac{2\tau_4^2}{\tau_3}} \sin \varphi \left[\gamma - j \left(\frac{\tau_4}{\tau_0} \right) \sin \varphi \right]} b_1 \quad (26)$$

where $\gamma = [(\omega - \omega_{\text{Res}-b})\tau_4 \sin \varphi - \cos \varphi]$. Using Eqs. (10), (18)-(19), and (26) the reflectivity and S'_{+1} can be written as

$$\frac{S_{-3}}{S_{+3}} = r = \frac{\frac{2\tau_4}{\tau_3} \sin \varphi \left[\gamma - j \left(\frac{\tau_4}{\tau_0} \right) \sin \varphi \right]}{\left[\gamma^2 - \frac{\tau_4}{\tau_0} \left(\frac{2\tau_4}{\tau_3} + \frac{\tau_4}{\tau_0} \right) \sin^2 \varphi - 1 \right] j + \gamma \sin \varphi \left(\frac{2\tau_4}{\tau_3} + \frac{2\tau_4}{\tau_0} \right)} \quad (27)$$

$$S'_{+1} = -r e^{-j\varphi} \left(S_{+1} - \sqrt{\frac{2}{\tau_1}} e^{-j\theta_1} a_1 \right) \quad (28)$$

where $\rho = 2\beta d$. The frequencies of the reflectivity peaks, given that $\tau_0 \gg \tau_3, \tau_4$, can be determined as

$$\omega_{\text{Res}_{1,2}} = \omega_{\text{Res}-b} + \frac{1}{\tau_4} \left(\frac{1}{\tan \varphi} \pm \frac{1}{\sin \varphi} \right). \quad (29)$$

From Eqs. (5), (15) and (28) the transmission spectrum of the CDF can be expressed as

$$D = \frac{S_{-2}}{S_{+1}} = \frac{\left(2 / \sqrt{\tau_1 \tau_2} \right) e^{j(\theta_1 - \theta_2)} \left[(1 - r \cos \rho) + j(r \sin \rho) \right] (j\tau_4 / \tau_0 \sin \varphi - \gamma)^{-1}}{j \left[(\omega - \omega_{\text{Res}-a}) + \frac{2r}{\tau_1} \sin \rho - \frac{1}{\tau_2 \tan \varphi} - \frac{\gamma}{\alpha \tau_2 \sin \varphi} \right] + \left[\frac{1}{\tau_0} + \frac{2}{\tau_1} - \frac{2r}{\tau_1} \cos \rho + \frac{(\tau_2 / \tau_0 + 1)}{\alpha \tau_2} \right]} \quad (30)$$

where $\alpha = \gamma^2 + \sin^2 \varphi (\tau_2 / \tau_0 + 1)^2$. Assuming that $\varphi \approx 0$, Eq. (30) can be much simplified as

$$D|_{\varphi \approx 0} = \frac{\left(2 / \sqrt{\tau_1 \tau_2} \right) e^{j(\theta_1 - \theta_2)} \left[(1 - r \cos \rho) + j(r \sin \rho) \right]}{j \left[(\omega - \omega_{\text{Res}-a}) + \frac{2r}{\tau_1} \sin \rho \right] + \left[\frac{2}{\tau_0} + \frac{2}{\tau_1} + \frac{1}{\tau_2} - \frac{2r}{\tau_1} \cos \rho \right]}. \quad (31)$$

Thus, given that $\omega_{\text{Res}-a} = \omega_{\text{Res}-b} = \omega_{\text{Res}}$ and $\tau_0 \gg \tau_1, \tau_2$ the drop efficiency at resonant frequencies can be expressed as

$$\eta|_{\omega = \omega_{\text{Res}_{1,2}}} = |D|^2|_{\omega = \omega_{\text{Res}_{1,2}}} = \frac{8k(1 - \cos \rho)}{8k^2(1 - \cos \rho) + 4k(1 - \cos \rho) + 1} \quad (32)$$

where $k = \tau_2 / \tau_1$. In this case, assuming $\rho = 2\beta d = (2n + 1)\pi$ for either ω_{Res_1} or ω_{Res_2} , where n is an integer, one can see that the channel drop efficiency of 100% will be obtained when $k = \tau_2 / \tau_1 = 1/4$. The dependence of the maximum of drop efficiency on k parameter is shown in Fig. 21-(a). Fig. 21-(b) shows the dependence of the maximum of drop efficiency on ρ parameter. The value of the cavities quality factor has an important role in the CDF performance.

On one hand, the cavities with high quality factor are necessary for implementation of three-port CDFs with narrow FWHM, which are the key element in WDM systems. On the other hand, at resonant frequencies and given that $\varphi \approx 0$, from Eq. (27) the reflectivity can be simplified to $r = \tau_3 / (\tau_3 + \tau_0)$ and in order to obtain 100% reflectivity, the condition $\tau_0 \gg \tau_3$ must be satisfied. Furthermore, concerning the sensitivity of the design and fabrication tolerance, the effect of the resonant frequency difference on the transmission spectrum is considerable. Assuming $\tau_0 \gg \tau_3$, $\omega_{\text{Res}-a} \neq \omega_{\text{Res}-b}$, $\rho = (2n + 1)\pi$ and $k = 1/4$ from Eq. (31), it can be shown that (Fasihi & Mohammadnejad, 2009b)

$$\eta_{\text{max}}|_{\omega_{\text{Res}_{1,2}}} = \frac{64}{\tau_1^2 (\omega_{\text{Res}-b} - \omega_{\text{Res}-a})^2 + 64} = \frac{4}{Q_1^2 \left(\frac{\omega_{\text{Res}-b}}{\omega_{\text{Res}-a}} - 1 \right)^2 + 4}. \quad (33)$$

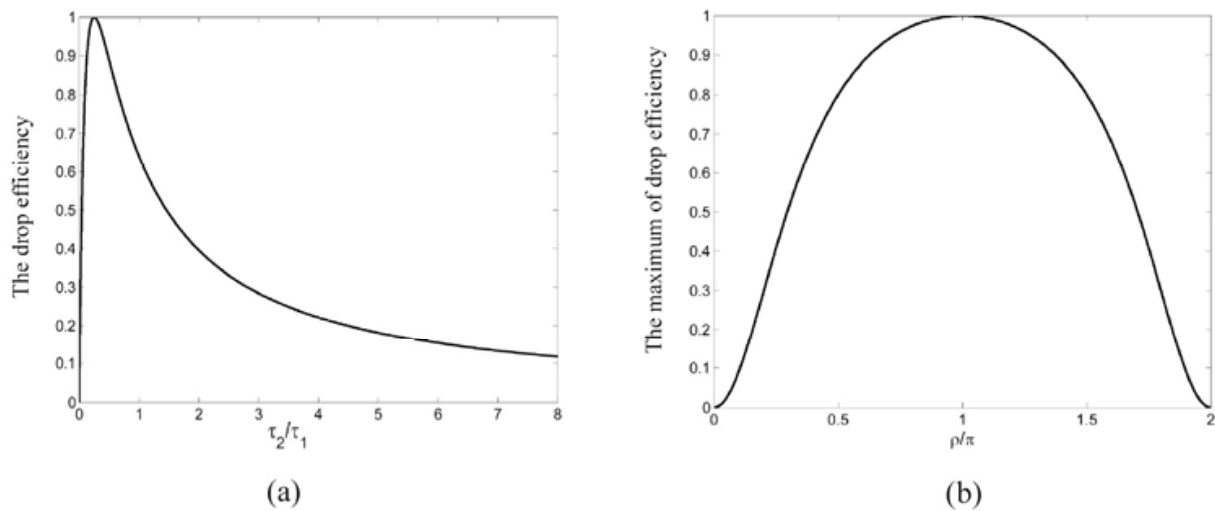


Fig. 21. (a) Dependence of drop efficiency at resonant frequencies on the ratio of decay rates τ_2 / τ_1 when $\rho = (2n + 1)\pi$. (b) Dependence of the maximum of drop efficiency on ρ / π (Fasihi & Mohammadnejad, 2009b)

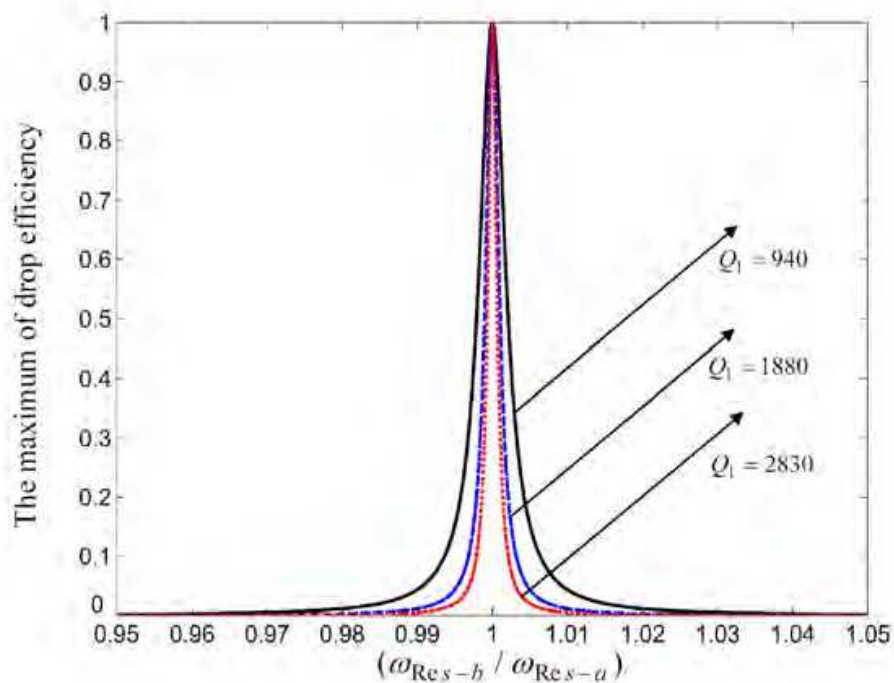


Fig. 22. Dependence of the maximum of drop efficiency on the frequency detuning factor $(\omega_{Res-b} / \omega_{Res-a})$.

This implies that by increasing the value of the quality factor, the detuning between the resonant frequencies, leads to the reduction in drop efficiency, and an advanced fabrication technology will be necessary. The drop efficiency as a function of the frequency detuning factor $(\omega_{Res-b} / \omega_{Res-a})$, is shown in Fig. 22 for modified HW1, HW2, and HW3 with $r_d = 0.04a$. Accordingly, by using appropriate structure with suitable values for the cavities quality factor, a narrowband three-port CDF with high transmission efficiency can be

achieved. We investigate the validity of the proposed PC coupled cavity based CDF by employing the FDTD method with PML absorbing boundary conditions. Fig. 23 shows the structure of the three-port CDF with wavelength-selective reflection feedback, in 2D-PC of square lattice composed of dielectric rods in air. All conditions are the same as the previous structures studied at section 2. The excitations are electromagnetic pulses with Gaussian envelope, which are applied to the bus waveguide from the top side. The field amplitudes are monitored at suitable locations at the bus and the drop waveguides. Fig. 24 shows the dispersion curve of the bus and the drop line-defect waveguides versus the wave vector component k along the defect.

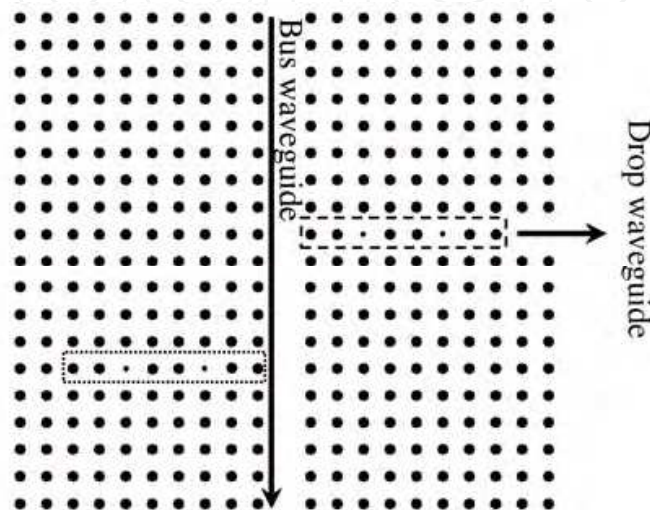


Fig. 23. The structure of three-port CDF with coupled cavity-based wavelength-selective reflection feedback, in 2D-PC of square lattice composed of dielectric rods in air. The dashed-line and the dotted-line rectangulars are the drop and the reflector sections, respectively.

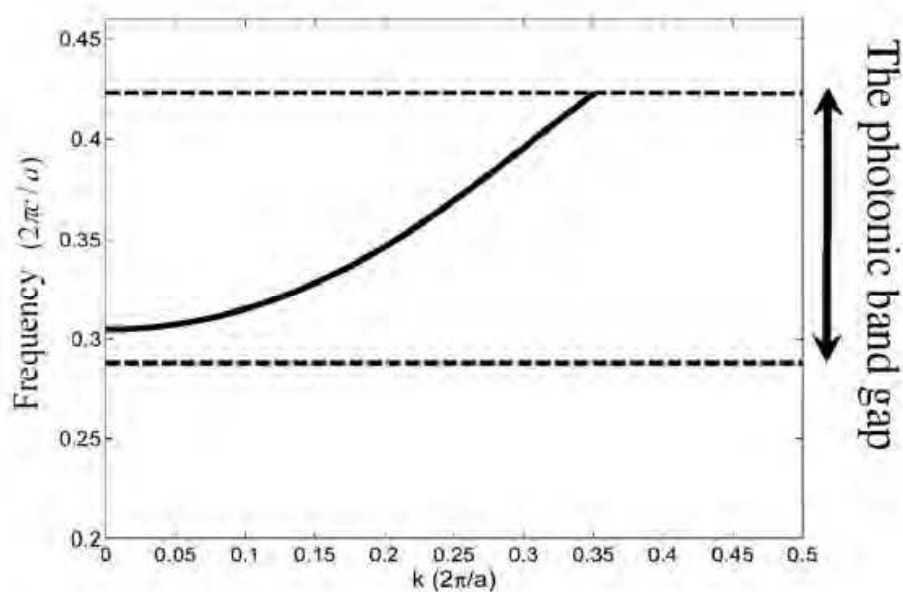


Fig. 24. Dispersion curve of the bus/drop line-defect waveguides versus the wave vector component k along the defect.

The resonant frequencies of the coupled cavities in the modified HW2 structure as a function of the coupled cavities radii are shown in Fig. 25. Given that the radii of the coupled cavities in the drop and reflector sections are set to $0.055a$, from Fig. 25, the corresponding resonant frequencies of the CDF coupled-cavities are $\omega_{\text{Res}_1} = 0.36076$ and $\omega_{\text{Res}_2} = 0.36573 (2\pi c / a)$. The τ_0 parameter, which is due to the internal loss of energy, is infinite in the desired 2D-PCs (Ren et al., 2006) and the total quality factors of the cavities are 1925. So, the condition $\tau_0 \gg \tau_3$ is satisfied and the perfect reflection can be realized. The condition $\tau_2 / \tau_1 = 1 / 4$ can be easily satisfied using the coupled mode theory (Kim et al., 2004). From Fig. 25 the guided mode has wave vectors $0.2325 \times (2\pi / a)$ and $0.2428 \times (2\pi / a)$ at ω_{Res_1} and ω_{Res_2} , respectively, and when the distance between the drop and reflector sections, d , is set to $14a$, the condition $\rho(\omega_{\text{Res}_1}) = 2\beta d = (2n + 1)\pi = 13\pi$ will be satisfied (in this case $\rho(\omega_{\text{Res}_2}) = 2\beta d = 13.59\pi$, which is not desired). Fig. 26-(a) shows the transmission spectra of the designed CDF calculated using the 2D-FDTD method. The simulated transmission spectrum through the drop waveguide (the dashed curve) represents that the proposed CDF has the ability of dropping a wavelength channel (at frequency ω_{Res_1}) with the dropping efficiency 0.95% and the spectral line-width $0.0014a$. Assuming the lattice constant $a = 0.56\mu\text{m}$, considering that in this case the wavelength corresponds to ω_{Res_1} is equal to 1550nm when $r_d = 0.055a$, the line-width is equal to 0.78nm . Fig. 26-(b) shows the transmission spectrum of the drop waveguide in dB. In this case, it can be seen that if channel spacing, $\delta\lambda$, is chosen as $\delta\lambda > (\lambda_{\text{Res}_1} - \lambda_{\text{Res}_2}) / 2 \approx 10\text{nm}$, the inter channel crosstalk is reduced to below -30 dB which shows very good ability for WDM devices in practical applications.

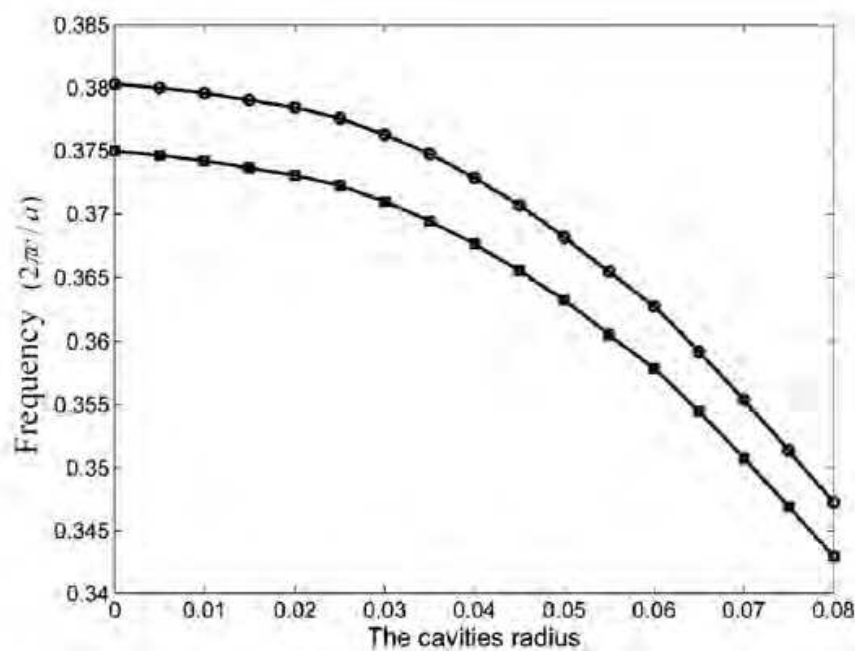


Fig. 25. Dependence of the resonant frequencies of the coupled cavities in the HW2 structure on the coupled cavities radii.

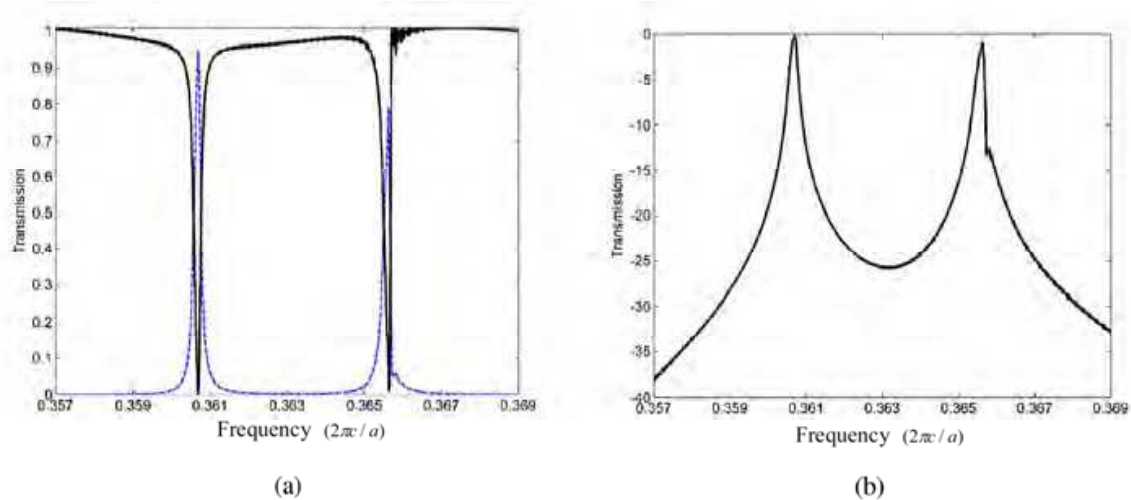


Fig. 26. Transmission spectra for the designed CDF calculated using the 2D-FDTD method. (a) The drop port (the dashed curve) and the bus port transmission spectrum (the solid curve). (b) The drop port transmission spectrum in dB (Fasihi & Mohammadnejad, 2009b).

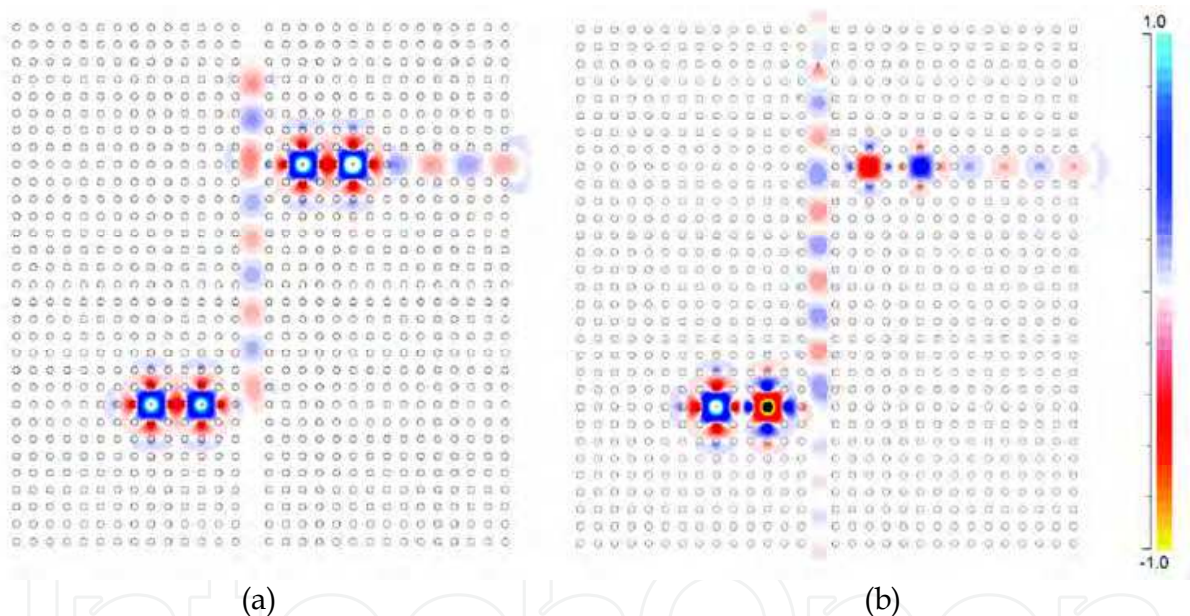


Fig. 27. The steady state wave propagation at the resonant frequencies of the designed CDF. (a) $\omega_{Res_1} = 0.36076 (2\pi c/a)$. (b) $\omega_{Res_2} = 0.36573 (2\pi c/a)$ (Fasihi & Mohammadnejad, 2009b)

The channel spacing can be reduced to $1nm$ for the $-15dB$ inter channel crosstalk. In a single cavity based CDF with reflector, the crosstalk with channel spacing of $20nm$ is between -18 to $-23 dB$ (Kuo et al., 2006). Fig. 27 shows the steady filed patterns at the resonant frequencies $\omega_{Res_1} = 0.36076$ and $\omega_{Res_2} = 0.36573 (2\pi c/a)$ at the bus and drop waveguides. For more optimal CDF design, the sizes of the rods between the cavities and the bus and drop waveguides, in both drop and reflector sections can be trimmed. In fact, by adjust tuning the resonant frequencies of the drop and reflector sections, further improve in CDF performance can be achieved and also the back reflection power into the input port, around the resonant frequencies, can be reduced. Even though, we don't use the additional

trimming in the design. Because the add operation is the “time-reversed” process of the channel drop operation, the tunneling-based channels add and drop operation can be combined into a compact form as shown in Fig. 28. The wavelength-selective reflection section locates in the central of the structure, and it ensures full power transfer between the bus waveguide and channel-add/drop sections. The top takes the narrow-band signal out of the bus waveguide while the bottom one couples signal from the transmitters into the bus-waveguide.

IntechOpen

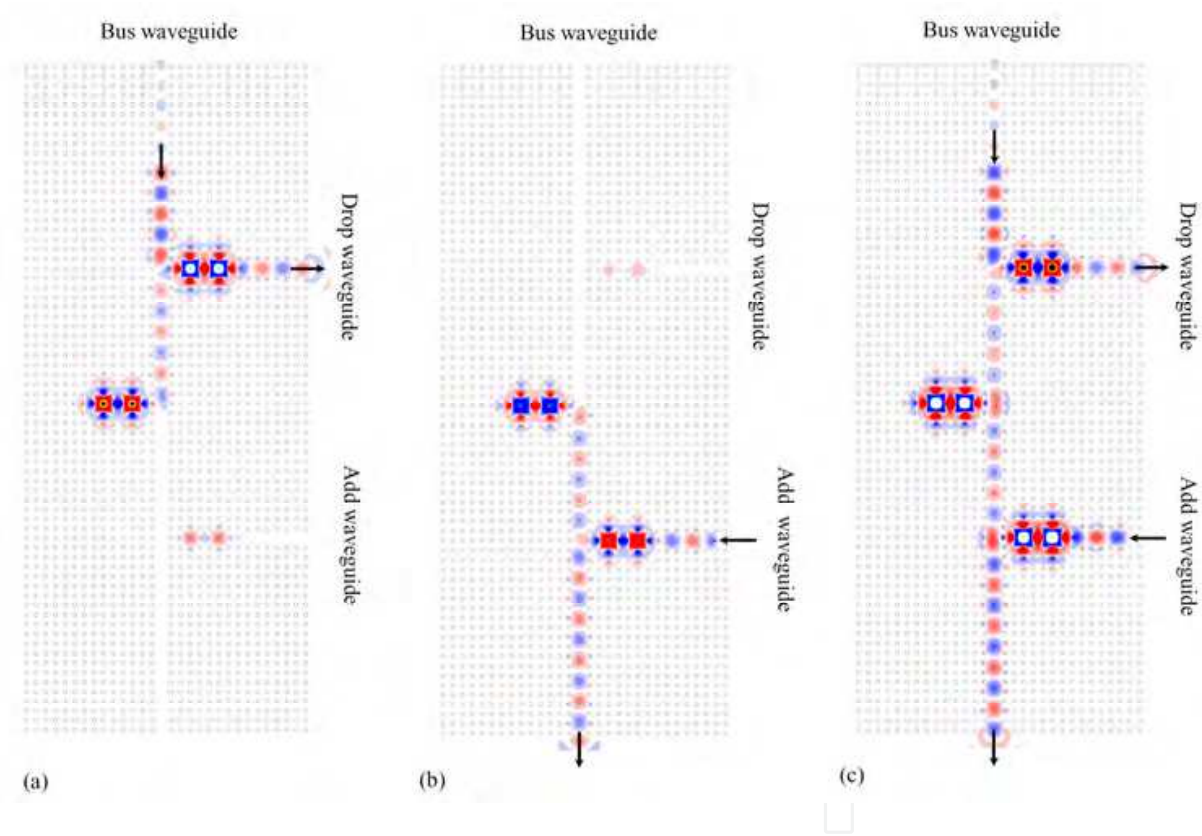


Fig. 28. The steady state wave propagation at the resonant frequency $\omega_{\text{Res}_1} = 0.36076 (2\pi c / a)$ of a passive channel add/drop filter designed based on proposed CDF. (a) Drop mechanism. (b) Add mechanism. (c) Add/drop mechanism.

4. Conclusions

In summary, the resonance frequencies and the field distributions of 2D-PC have been investigated. PC hybrid waveguides with quasi-flat and Lorentzian transmission spectrum were analyzed and modeled by using FDTD and CMT methods. The theoretical results derived by CMT were in good agreement with FDTD simulation results. It was shown that when the phase-shift of the electromagnetic waves traveling between two adjacent PC coupled cavities (φ), is close to $(k+1/2)\pi$, the transmission spectrum of the hybrid waveguide is quasi-flat. A modified HW3 with extra rods in both ends of the CCW and Lorentzian transmission spectrum was proposed, which can be used in implementation of WDM filters. It was shown that in this case φ is close to zero. Transmission of ultra-short pulses through the hybrid waveguide was also investigated. A low cross-talk and wideband PC waveguide intersection design based on two orthogonal hybrid waveguides in a crossbar configuration was proposed. Also, it has been shown that when $\varphi \approx (k+1/2)\pi$, optimum performance results for the intersection can be achieved. In addition, it has been clearly proved that simultaneous crossing of ultra-short pulses through the intersection is possible with negligible interference. The transmission of a 200-fs pulse at 1550 nm was simulated by using the FDTD method, and the transmitted pulse showed negligible cross-talk and very little distortion. A three-port high efficient CDF with a coupled cavity-based wavelength-selective reflector, which can be used in WDM optical communication systems, was proposed. The CMT was employed to derive the necessary conditions for achieving 100% drop efficiency. The FDTD simulation results of proposed CDF which was implemented in 2D-PC, showed that the analysis was valid. The simulation results show that the designed CDF has a line-width of 0.78nm at the center wavelength 1550nm , and also a multi-channel CDF with channel spacing around 10nm (1nm) with inter-channel crosstalk below -30dB (-15dB) is possible. These characteristics make the proposed CDF suitable for use in WDM optical communication systems.

5. References

- Chen, C. C. Chen, C. Y. Wang, W. K. Huang, F. H. Lin, C. K. Chiu, W. Y. and Chan, Y. J. (2005). Photonic Crystal Directional Couplers Formed by InAlGaAs Nano-Rods. *Opt. Express*, 13, pp. 38–43.
- Ding, W. Chen L. and Liu, S. (2004). Localization properties and the effects on multi-mode switching in discrete mode CCWs. *Optics Communications*, 248, pp. 479–484.
- Fan, S. Villeneuve, P. R. Joannopoulos, J. D. Khan, M. J. Manolatou, C. and Haus, H. A. (1999). Theoretical analysis of channel drop tunneling processes. *Phys. Rev., B* (59), pp. 15882–15892.
- Fasihi, K. and Mohammadnejad, S. (2009a). Orthogonal Hybrid Waveguides: an Approach to Low Cross-talk and Wideband Photonic Crystal Intersections Design. *IEEE J. Lightw. Technol.*, 27, pp. 799–805.

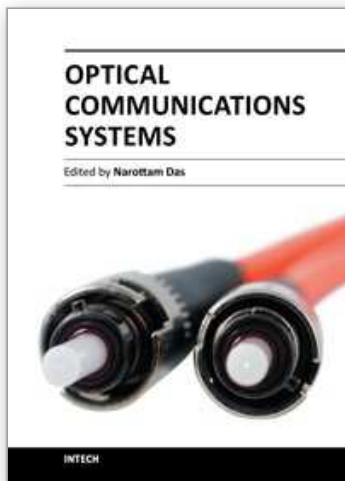
- Fasihi, K. and Mohammadnejad, S. (2009b). Highly efficient channel-drop filter with a coupled cavity-based wavelength-selective reflection feedback. *Opt. Express.*, 173, pp. 8983–8997.
- Fan, S. Villeneuve, P. R. Joannopoulos, J. D. and Haus, H. A. (1998). Channel drop filters in photonic crystals. *Opt. Express.* 3, 4-11.
- Fujisawa, T. and Koshiba, M. (2006). Finite-Element Modeling of Nonlinear Mach-Zehnder Interferometers Based on Photonic-Crystal Waveguides for All-optical Signal Processing. *IEEE J. Lightw. Technol.*, 24, pp. 617–623.
- Haus, H. A. (1984). *Waves and Field in Optoelectronics* (Prentice-Hall).
- Jin, C. Fan, S. Han, S. and Zhang, D. (2003). Reflectionless multichannel wavelength demultiplexer in a transmission resonator configuration. *J. Quantum Electron.* 39, 160-165.
- Joannopoulos, J. D. Johnson, S. G. Winn, J. N. and Meade, R. D. (2008). *Photonic Crystal: Molding the Flow of Light*. Princeton, Princeton Univ. Press.
- Johnson, S. J. Manolatu, C. Fan, S. Villeneuve, P. R. Joannopoulos, J. D. and Haus, H. A. (1998). Elimination of Crosstalk in Waveguide Intersections," *Opt. Lett.*, vol. 23, pp. 1855–1857.
- Kim, S. park, I. Lim, H. and Kee, C. (2004). Highly efficient photonic crystal-based multi-channel drop filters of three-port system with reflection feedback. *Opt. Express.* 12, 5518-5525.
- Koshiba, M. (2001). Wavelength Division Multiplexing and Demultiplexing With Photonic Crystal Waveguide Coupler. *IEEE J. Lightw. Technol.*, 19, pp. 1970–1975.
- Kuo, C. W. Chang, C. F. Chen, M. H. Chen, S. Y. and Wu, Y. D. (2006). A new approach of planar multi-channel wavelength division multiplexing system using asymmetric super-cell photonic crystal structures. *Opt. Express.* 15, 198-206.
- Loncar, M. Nedeljkovic, D. Doll, T. Vuckovic, J. Scherer, A. and Pearsall, T. P. (2000). Waveguiding in planar photonic crystals. *Appl. Phys. Lett.*, 77, pp. 1937–1939.
- Lan, S. and Ishikawa, H. (2002). broadband waveguide intersections with low cross talk in photonic crystal circuits. *Opt. Lett.*, vol. 27, pp. 1567–1569.
- Li, Z. Chen, H. Chen, J. Yang, F. Zheng H. and Feng, S. (2007). A proposal for low cross-talk square-lattice photonic crystal waveguide intersection utilizing the symmetry of waveguide modes. *Optics Communications.*, vol. 273, pp. 89–93.
- Liu, T. Fallahi, M. Mansuripour, M. Zakharian, A. R. and Moloney, V. (2005). Intersection of nonidentical optical waveguides based on photonic crystals. *Opt. Lett.*, vol. 30, pp. 2409–2411.
- Liu, C. Y. and Chen, L. W. (2004). Tunable photonic-crystal waveguide Mach-Zehnder interferometer achieved by nematic liquid-crystal phase modulation. *Opt. Express.*, 12(12) pp. 2616–2624.
- Martinez, A. Griol, A. Sanchis, P. and Marti, J. (2003). Mach-Zehnder interferometer employing coupled-resonator optical waveguides. *Opt. Lett.*, 28, no. 6, pp. 405–407.

- Manolatou, C. Khan, M. J. Fan, S. Villeneuve, P. R. Haus, H. A. and Joannopoulos, J. D. (1999). Coupling of modes analysis of resonant channel add-drop filters. *IEEE J. Quantum Electron.* 35, 1322 -1333.
- Mekis, A. Meier, M. Dodabalapur, A. Slusher, R. E. and Joannopoulos, J. D. (1999). Lasing mechanism in two-dimensional photonic crystal lasers. *Appl. Phys. A: Materials Science & Processing*, 69, pp. 111-114.
- Mekis, A. Chen, J. C. Kurland, I. Fan, S. Villeneuve, P. R. and Joannopoulos, J. D. (1996). High transmission through sharp bends in photonic crystal waveguides," *Phys. Rev. Lett.*, 77, pp. 3787-3790.
- Min, B. K. Kim, J. E. and Park, H. Y. (2004). Channel drop filters using resonant tunneling processes in two dimensional triangular lattice photonic crystal slabs. *Opt. Commun.* 237, 59-63.
- Niemi, T. H. Frandsen, L. Hede, K. K. Harpøth, A. Borel, P. I. and Kristensen, M. (2006). Wavelength-Division Demultiplexing Using Photonic Crystal Waveguides. *IEEE Photon. Technol. Lett.*, 18, pp. 226-228.
- Noda, S. Chutinan, A. and Imada, M. (2000). Trapping and emission of photons by a single defect in a photonic bandgap structure. *Nature*. 407, 608-610.
- Notomi, M. Shinya, A. Mitsugi, S. Kuramochi, E. and Ryu, H. (2004). "Waveguides, resonators and their coupled elements in photonic crystal slabs. *Opt. Express*. 12, 1551-1561.
- Ren, H. Jiang, C. Hu, W. Gao, M. and Wang, J. (2006). Photonic crystal channel drop filter with a wavelength-selective reflection micro-cavity. *Opt. Express*. 14, 2446-2458.
- Sheng, L. X. Wen C. X. and Sheng, L. (2005). Analysis and engineering of coupled cavity waveguides based on coupled-mode theory. *Chin. Phys. Soc. and IOP Publishing Ltd.*, 14, pp. 2033-2040.
- Shin, M. H. Kim, W. J. Kuang, W. Cao, J. R. Yukawa, H. Choi, S. J. O'Brien, J. D. Dapkus, P. D. and Marshall, W. K. (2004). Two-dimensional photonic crystal Mach-Zehnder interferometers. *Appl. Phys. Lett.*, 84, no. 4, pp. 460-462.
- Song, B. Asano, T. Akahane, Y. and Noda, S. (2005). Role of interfaces in hetero photonic crystals for manipulation of photons. *Phys. Rev. B* 71, 195101-19105.
- Tekeste M. Y. and Yarrison-Rice, J. M. (2006). High efficiency photonic crystal based wavelength demultiplexer. *Opt. Express*. 14, 7931-7942.
- Villeneuve, P. R. Fan, S. and Joannopoulos, J. D. (1996). Microcavities in photonic crystals: Mode symmetry, tunability, and coupling efficiency. *Phys. Rev.*, vol. B 54, pp. 7837-7842.
- Yanik, M. F. Altug, H. Vuckovic, J. and Fan, S. (2004). Submicrometer All-Optical Digital Memory and Integration of Nanoscale Photonic Devices without Isolator. *IEEE J. Lightw. Technol.*, 22, pp. 2316-2322.
- Yanik, M. F. Fan, S. Soljačić, M. and Joannopoulos, J. D. (2003). All-optical transistor action with bistable switching in a photonic crystal crosswaveguide geometry. *Opt. Lett.*, 28(24), pp. 2506-2508.
- Yariv, A. Xu, Y. Lee, R. and Scherer, A. (1999). "Coupled-resonator optical waveguide: a proposal and analysis," *Opt. Lett.*, (24), pp. 711-713.

- Zhang Z. and Qiu, M. (2004). Coupled-mode analysis of a resonant channel drop filter using waveguides with mirror boundaries. *J. Opt. Soc. Am. B* 23, 104-113.
- Zhang Z. and Qiu, M. (2005). Compact in-plane channel drop filter design using a single cavity with two degenerate modes in 2D photonic crystal slabs. *Opt. Express*. 13, 2596-2604.

IntechOpen

IntechOpen



Optical Communications Systems

Edited by Dr. Narottam Das

ISBN 978-953-51-0170-3

Hard cover, 262 pages

Publisher InTech

Published online 07, March, 2012

Published in print edition March, 2012

Optical communications systems are very important for all types of telecommunications and networks. They consist of a transmitter that encodes a message into an optical signal, a channel that carries the signal to its destination, and a receiver that reproduces the message from the received optical signal. This book presents up to date results on communication systems, along with the explanations of their relevance, from leading researchers in this field. Its chapters cover general concepts of optical and wireless optical communication systems, optical amplifiers and networks, optical multiplexing and demultiplexing for optical communication systems, and network traffic engineering. Recently, wavelength conversion and other enhanced signal processing functions are also considered in depth for optical communications systems. The researcher has also concentrated on wavelength conversion, switching, demultiplexing in the time domain and other enhanced functions for optical communications systems. This book is targeted at research, development and design engineers from the teams in manufacturing industry; academia and telecommunications service operators/providers.

How to reference

In order to correctly reference this scholarly work, feel free to copy and paste the following:

Kiazand Fasihi (2012). Design and Modeling of WDM Integrated Devices Based on Photonic Crystals, Optical Communications Systems, Dr. Narottam Das (Ed.), ISBN: 978-953-51-0170-3, InTech, Available from: <http://www.intechopen.com/books/optical-communications-systems/design-and-modeling-of-wdm-integrated-devices-based-on-photonic-crystals->

INTECH
open science | open minds

InTech Europe

University Campus STeP Ri
Slavka Krautzeka 83/A
51000 Rijeka, Croatia
Phone: +385 (51) 770 447
Fax: +385 (51) 686 166
www.intechopen.com

InTech China

Unit 405, Office Block, Hotel Equatorial Shanghai
No.65, Yan An Road (West), Shanghai, 200040, China
中国上海市延安西路65号上海国际贵都大饭店办公楼405单元
Phone: +86-21-62489820
Fax: +86-21-62489821

© 2012 The Author(s). Licensee IntechOpen. This is an open access article distributed under the terms of the [Creative Commons Attribution 3.0 License](#), which permits unrestricted use, distribution, and reproduction in any medium, provided the original work is properly cited.

IntechOpen

IntechOpen